

NOAA Technical Memorandum OAR ARL-243

**METEOROLOGICAL MEASUREMENTS DURING THE URBAN 2000/VTMX
FIELD STUDY**

Kirk L. Clawson
Gennaro H. Crescenti

Field Research Division
Idaho Falls, Idaho

Air Resources Laboratory
Silver Spring, Maryland
May 2002



**UNITED STATES
DEPARTMENT OF COMMERCE**

**Donald L. Evans
Secretary**

**NATIONAL OCEANIC AND
ATMOSPHERIC ADMINISTRATION**

**VADM Conrad C. Lautenbacher, Jr.
Under Secretary for Oceans
and Atmosphere/Administrator**

**Oceanic and Atmospheric
Research Laboratories**

**David L. Evans
Director**

NOTICE

This report was prepared as an account of work sponsored by an agency of the United States Government. Neither the United States Government nor any agency thereof, or any of their employees, makes any warranty, expressed or implied, or assumes any legal liability or responsibility for any third party's use, or the results of such use, of any information, apparatus, product or process disclosed in this report, or represents that its use by such third party would not infringe privately owned rights. Mention of a commercial company or product does not constitute an endorsement by NOAA/OAR. Use of information from this publication concerning proprietary products or the tests of such products for publicity or advertising is not authorized.

CONTENTS

	<u>Page</u>
Abstract	viii
Introduction	1
3-D Sonic Anemometers	3
Data Processing and Quality Control	6
Summary Statistics	7
Sonic Anemometer Comparison	9
Upper-air and Standard Surface Meteorology Station	11
10-m Tower	14
Sodar and Radar	19
Intensive Observation Period (IOP) Case Studies	29
IOP 1	31
IOP 2	33
IOP 3	34
IOP 4	35
IOP 5	37
IOP 6	38
IOP 7	39
IOP 8	40
IOP 9	41
IOP 10	41
Acknowledgments	44
References	45

FIGURES

	<u>Page</u>
Figure 1. Oblique aerial photograph of downtown Salt Lake City looking towards the northeast with the Wasatch Mountains in the background. Photograph from Don Green Photography, Salt Lake City, Utah.	2
Figure 2. Sonic anemometers mounted on the LLNL mobile laboratory mast. The ATI anemometer is at the top of the mast with the GILL mounted below. A rising quarter moon can be seen between the two anemometers.	3
Figure 3. Sonic anemometers mounted on the LLNL mobile laboratory mast stationed in the City Centre (Chamber of Commerce) parking lot. The City Centre building can be seen to the left, while the City building tower can be seen at right. The tower is located across the street to the south of the parking lot.	4
Figure 4. Aerial photograph of the City Centre parking lot surrounding buildings. Approximate location of the sonic anemometer mast is indicated by X. Photo courtesy USGS.	5
Figure 5. Meteorological tower and associated instrumentation.	11
Figure 6. Doppler sodar and radar wind profiler.	11
Figure 7. Location of the 10-m tower, sodar, and radar profiler at Raging Waters (yellow box) relative to the downtown SF ₆ atmospheric tracer release site (blue star), in relationship to the Salt Lake Valley.	12
Figure 8. Raging Waters vista photos.	13
Figure 9. Wind rose for 10-m tower.	14
Figure 10. Time series of tower-based vector wind speed, vector wind direction, standard deviation of the wind direction (σ_θ), air temperature, relative humidity, and battery voltage from October 1-8, 2000.	15
Figure 11. Time series of tower-based vector wind speed, vector wind direction, standard deviation of the wind direction (σ_θ), air temperature, relative humidity, and battery voltage from October 8-15, 2000.	16
Figure 12. Time series of tower-based vector wind speed, vector wind direction, standard deviation of the wind direction (σ_θ), air temperature, relative humidity, and battery voltage from October 15-22, 2000.	17

Figure 13. Time series of tower-based vector wind speed, vector wind direction, standard deviation of the wind direction (σ_θ), air temperature, relative humidity, and battery voltage from October 22-29, 2000.	18
Figure 14. Representation of the 120-transducer phased-array Doppler sodar antenna. Functional transducers are depicted by \circ while nonfunctional transducers are depicted by \bullet . ..	20
Figure 15. Sodar data availability as a function of time and height.	22
Figure 16. Average sodar scalar wind speed as a function of time and height.	22
Figure 17. Sodar vector wind speed as a function of time and height.	23
Figure 18. Sodar wind persistence as a function of time and height.	23
Figure 19. Radar (mode 1) data availability as a function of time and height.	24
Figure 20. Radar (mode 2) data availability as a function of time and height.	24
Figure 21. Radar (mode 1) scalar wind speed as a function of time and height.	25
Figure 22. Radar (mode 2) scalar wind speed as a function of time and height.	25
Figure 23. Radar (mode 1) vector wind speed as a function of time and height.	26
Figure 24. Radar (mode 2) vector wind speed as a function of time and height.	26
Figure 25. Radar (mode 1) wind persistence as a function of time and height.	27
Figure 26. Radar (mode 2) wind persistence as a function of time and height.	27
Figure 28. Sonic anemometer data averaged for 30-min time periods for wind speed, wind direction, virtual temperature, kinematic momentum flux, and kinematic sensible heat flux. Black is the ATI sonic anemometer and read is the Gill sonic anemometer.	32
Figure 28. Tower, sodar, and radar wind vectors during IOP 2.	34
Figure 29. Tower, sodar, and radar wind vectors during IOP 3.	35
Figure 30. Tower, sodar, and radar wind vectors during IOP 4.	36
Figure 31. Tower, sodar, and radar wind vectors during IOP 5.	37
Figure 32. Tower, sodar, and radar wind vectors during IOP 6.	38

Figure 33. Tower, sodar, and radar wind vectors during IOP 7.	39
Figure 34. Tower, sodar, and radar wind vectors during IOP 8.	40
Figure 35. Tower, sodar, and radar wind vectors during IOP 9.	42
Figure 36. Tower, sodar, and radar wind vectors during IOP 10.	43

TABLES

	<u>Page</u>
Table 1. Sonic anemometer data files.	5
Table 2. Average and variance of the parameters included in the .FLX files for the ATI and GILL sonic anemometers.	10
Table 3. Summary of URBAN 2000/VTMX IOPs.	29
Table 4. Sonic anemometer summary statistics for each IOP.	30

ABSTRACT

In October 2000, scientists funded by the U. S. Department of Energy's (DOE) Chemical and Biological National Security Program (CBNP) conducted a comprehensive field tracer study in an urban environment. The study, known as URBAN 2000, was conducted in Salt Lake City, Utah. The study was designed to measure flow and dispersion at multiple scales, thereby allowing a nested system of atmospheric dispersion models to be tested and evaluated under identical meteorological conditions. A set of atmospheric tracer experiments was conducted to investigate transport and dispersion around a single downtown building, through the downtown area and into the suburban area to the northwest of downtown. A spatially dense array of meteorological measurements was deployed in support URBAN 2000, both in the downtown area and in the suburban area. In addition, the study area was extended beyond the suburban scale by embedding URBAN 2000 in DOE's concurrent region-wide Vertical Transport and Mixing (VTMX) tracer and meteorological study. Both the URBAN 2000 and VTMX studies were focused on investigations of the nocturnal boundary layer in stable to neutral atmospheric conditions.

The URBAN 2000 and VTMX experiments were cooperative multi-agency efforts. Under the URBAN 2000 funding umbrella, NOAA's Air Resources Laboratory (ARL) Field Research Division (FRD) deployed meteorological instrumentation at two different sites to support both studies. Two sonic anemometers were deployed by FRD in downtown Salt Lake City during intensive observation periods (IOP) to characterize atmospheric turbulence in the vicinity of the sulfur hexafluoride (SF_6) atmospheric tracer release site. A 10-m meteorological tower, a phased array Doppler sodar, and a radar wind profiler were also deployed for a three-week period at a site approximately 5 km southwest of downtown Salt Lake City. Many other sites were instrumented with meteorological equipment by other groups participating in the studies. The analysis of all these data sets is beyond the scope of this report. Only the meteorological data acquired by FRD is described herein.

INTRODUCTION

In the autumn of 2000, scientists funded by the U. S. Department of Energy's (DOE) Chemical and Biological National Security Program (CBNP) of the National Nuclear Security Administration conducted a comprehensive field tracer study in an urban environment. That study has come to be known as URBAN 2000. The study was designed to measure flow and dispersion at multiple scales, thereby allowing a nested system of atmospheric dispersion models to be tested and evaluated under identical meteorological conditions (Allwine et al., 2002). In retrospect, the findings from URBAN 2000 have become quite useful to homeland security research. CBNP is an applied research and development program that focuses emerging science and technology on countering the challenging threat of chemical and biological weapons attacks on civilian populations (U. S. DOE, 2001). To adequately plan, train and respond to potential attacks, atmospheric models are being developed, tested, and evaluated as part of CBNP to provide users in intelligence, law enforcement, and emergency management with an integrated set of computer-based modeling tools (Allwine et al., 2002).

URBAN 2000 was conducted in Salt Lake City, Utah during October 2000. Salt Lake City has a rather complicated downtown urban building geometry (Fig. 1). Atmospheric tracer experiments were conducted to investigate transport and dispersion around a single downtown building, through the downtown area and into the suburban area to the northwest of downtown. A spatially dense array of meteorological instruments was deployed in support of URBAN 2000, both in the downtown area and in the suburban area. In addition, the study area was extended beyond the suburban scale by embedding URBAN 2000 in DOE's concurrent region-wide Vertical Transport and Mixing (VTMX) tracer and meteorological study (Doran et al., 2002). Both the URBAN 2000 and VTMX studies were designed to characterize the nocturnal boundary layer in stable to neutral atmospheric conditions and to investigate flow and dispersion in such conditions.

The URBAN 2000 and VTMX programs had complementary objectives. While the URBAN experiment focused on the urban nocturnal boundary layer, VTMX focused on the valley-wide nocturnal boundary layer. Our understanding of vertical transport and mixing processes in the lowest few kilometers of the atmosphere is very limited during periods of light winds and weak turbulence. These conditions frequently occur at night or during stagnation episodes in the winter. Important aspects of air quality modeling and weather forecasting are adversely affected by our inability to quantify these processes. In addition, the necessary data needed to test and refine these models is inadequate. The upward and downward movements of air parcels in stable and residual layers and the interactions between adjacent layers are particularly difficult processes to characterize. A quantitative description of the atmosphere during morning and evening transition periods is also difficult to formulate. Furthermore, heterogeneous land/water surfaces and complex terrain compromise our ability properly characterize vertical transport and mixing processes.

To address these issues, the DOE's Environmental Meteorology Program (EMP) developed a research study to investigate vertical transport and mixing (VTMX) processes in the lower atmosphere (Doran et al., 2002). The goals of the VTMX program are: 1) to increase the understanding of the mechanisms responsible for vertical transport and mixing, 2) to improve the

ability to measure quantities required for this understanding; and 3) to develop improved treatments of vertical transport and mixing for use in conceptual and numerical models.

The Salt Lake Valley of northern Utah was chosen as the study site for VTMX. The Wasatch Mountains to the east, and Oquirrh Mountains to the west, often contribute to the development of cold pools in which colder air is trapped on the valley floor while warmer air is found aloft. Vertical transport and mixing processes during these conditions can be especially difficult to describe. Flows over the mountains and out of the canyons as well as thermally driven winds between the Great Salt Lake and the valley floor may generate wind shear and atmospheric waves. These, in turn, can modify the vertical structure of the atmospheric boundary layer.

Both the URBAN 2000 and VTMX experiments were cooperative multi-agency efforts. Under the URBAN 2000 funding umbrella, NOAA's Air Resources Laboratory (ARL) Field Research Division (FRD) deployed meteorological instrumentation at two different sites to support both studies. Two sonic anemometers were deployed by FRD in downtown Salt Lake City during intensive observation periods (IOP) to characterize atmospheric turbulence in the vicinity of the sulfur hexafluoride (SF_6) atmospheric tracer release site. A 10-m meteorological tower, a phased array Doppler sodar, and a radar wind profiler were also deployed for a three-week period at a site approximately 5 km southwest of downtown Salt Lake City. Many other sites were instrumented with meteorological equipment by other groups participating in the studies. However, an additional effort beyond the scope of this report will be necessary to assemble and analyze the multiple data sets for a more complete understanding of the nocturnal meteorology of the Salt Lake Valley. The focus of this report is to summarize the meteorological data acquired by FRD.



Figure 1. Oblique aerial photograph of downtown Salt Lake City looking towards the northeast with the Wasatch Mountains in the background. Photograph from Don Green Photography, Salt Lake City, Utah.

3-D SONIC ANEMOMETERS

Two three-dimensional sonic anemometers were placed in the parking lot of the City Centre (Chamber of Commerce) building located at 175 East 400 South, Salt Lake City (Fig. 2). They were deployed only on the nights when the SF₆ or perfluorocarbon atmospheric tracers were released. The sonic anemometers used in the study were designated ATI and GILL. The ATI sonic anemometer (model SAT-211/3K) was a “K-style” probe fashioned after the design of Kaimal and manufactured by Applied Technologies, Inc., in Boulder, Colorado. The Gill sonic anemometer was the Windmaster Pro model, manufactured by Gill Instruments, Ltd., in Lymington, Hampshire, United Kingdom.

The sonic anemometers were mounted on a mast attached to the mobile laboratory facility (motor home) provided by Lawrence Livermore National Laboratory (LLNL). The motor home was placed in the parking lot on the west side of the City Centre building (Fig. 3). More specifically, the motor home was placed approximately 50 m west of the west side of the building on an imaginary line that ran due west in line with the north wall of the building into the parking lot. Starting with IOP 4, the motor home was placed approximately 2.5-3.0 m north of that line. An aerial photograph (Fig. 4) shows the parking lot and its relationship to surrounding buildings. As can be seen, the sonic anemometers were placed well within the distorted flow of the neighboring buildings. The GPS-determined location was 40° 45.698' N, 111° 53.230' W. The orientation of the sonic anemometer mounting arms was 180 deg, facing into the prevailing wind direction. The Gill was mounted 6.90 m above ground level (AGL), while the ATI was mounted 9.81 m AGL.

The data from each sonic anemometer were recorded at a rate of 10 Hz using custom designed data acquisition software on two separate computers running Microsoft DOS. The data were stored in binary format with a filename of the form *XDDDTTTT.RAW*, where *X=A* for ATI or *X=G* for Gill, *DDD* is the day of year, and *TTTT* is the time (HHMM, MDT). The raw data file name indicates the beginning time of each file and contains up to 30 min of data. A total of 90 data files was recorded



Figure 2. Sonic anemometers mounted on the LLNL mobile laboratory mast. The ATI anemometer is at the top of the mast with the GILL mounted below. A rising quarter moon can be seen between the two anemometers.

for each sonic anemometer. These files, together with the associated IOP, are listed in Table 1. Each data acquisition program was manually and simultaneously started to within 0.25 s of each other initially, but the sonic anemometer and computer clocks could have drifted from each other during the approximately 6-hr operation. The only time stamp for a given data file is the filename. For accurate simultaneous operation of tower-mounted sonic anemometers, the data acquisition must be synchronized on an acquisition pulse. This procedure was not followed for this experiment.



Figure 3. Sonic anemometers mounted on the LLNL mobile laboratory mast stationed in the City Centre (Chamber of Commerce) parking lot. The City Centre building can be seen to the left, while the City building tower can be seen at right. The tower is located across the street to the south of the parking lot.

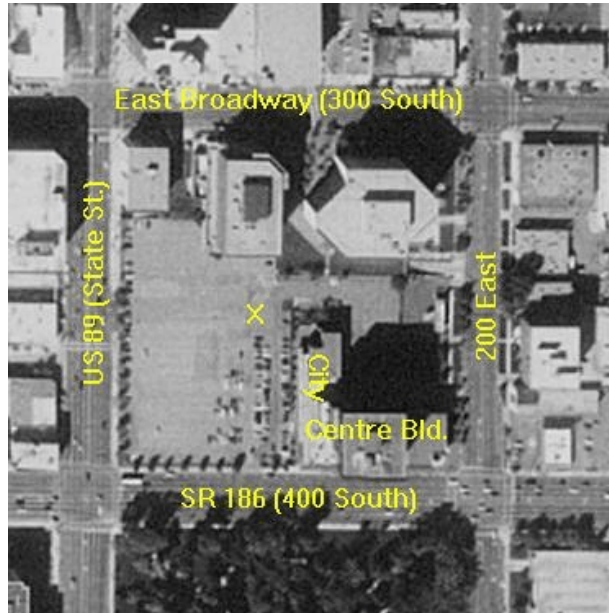


Figure 4. Aerial photograph of the City Centre parking lot surrounding buildings. Approximate location of the sonic anemometer mast is indicated by X. Photo courtesy USGS.

Table 1. Sonic anemometer data files.

IOP	. RAW File Names (Day of Year and Time, MDT)	Number of Files
1	2762208, 2762230, 2762300, 2762330, 2770000, 2770030, 2770100, 2770130, 2770200, 2770230, 2770300, 2770330, 2770400	13
2	2802146, 2802200, 2802230, 2802300, 2802330, 2810000, 2810030, 2810100, 2810130, 2810200, 2810230, 2810300, 2810330, 2810400, 2810430, 2810500, 2810530	17
4	2830005, 2830030, 2830100, 2830130, 2830200, 2830230, 2830300, 2830330, 2830400, 2830430, 2830500	11
5	2890013, 2890030, 2890100, 2890130, 2890200, 2890230, 2890300, 2890330, 2890400, 2890430, 2890500	11
7	2920000, 2920030, 2920100, 2920130, 2920200, 2920230, 2920300, 2920330, 2920400, 2920430, 2920500, 2920530	12
9	2942104, 2942130, 2942200, 2942230, 2942300, 2942330, 2950000, 2950030, 2950100, 2950130, 2950200, 2950230, 2950300	13
10	3000008, 3000030, 3000100, 3000130, 3000200, 3000230, 3000300, 3000330, 3000400, 3000430, 3000500, 3000530, 3000600	13

Data Processing and Quality Control

The .RAW data files were subsequently processed and converted into comma-separated ASCII (.CSV) and space delimited ASCII (.DAT) files after completion of the study. The .CSV and .DAT files were named in the same manner as the .RAW files, and subsequently submitted to the public experiment database. The .RAW files were not included in the data dissemination because they are binary files and they were not subjected to stringent post-processing procedures. The .CSV and .DAT data files have the same format, with the exception that the .CSV files have a header row that describes each column. The four data parameters included are:

1. Vertical wind component (w), units of m s^{-1} , positive from the surface upward;
2. Horizontal wind component (u), units of m s^{-1} , positive from west to east;
3. Horizontal wind component (v), units of m s^{-1} , positive from south to north; and
4. Virtual air temperature, units of $^{\circ}\text{C}$

A time stamp was also not included in the .CSV and .DAT files because the anemometers were not synchronized on an acquisition pulse. Thus, each data point from either sonic anemometer was recorded at approximately the same time, but not precisely at the same time. Slight differences in total number of data points were observed in every 30-min data file. A 30-min data file should have 18,000 data points. Actual number of data points for a full 30-min file ranged from 18001 to 18003. The resulting error rate of approximately 0.01% was very small. The difference in time due to the manual setting of the computer clocks and the manual initialization of the recording programs was obviously larger than the sonic anemometer clock error.

Well established and documented algorithms were used on the 10-Hz sonic anemometer data for quality control measures and to calculate 30-min summary statistics, which are explained later. During the quality control process, five of the ATI sonic anemometer data files were found to contain one scan of spurious data each and one file was found to contain two scans of spurious data. These data were subsequently purged from the .CSV and .DAT data files. If the direct scan by scan comparison of the GILL and ATI sonic anemometer data is to be attempted in the future, it is important to know which scans were deleted. The file names and the deleted scan numbers are:

A2802146.CSV or .DAT 180
A2802330.CSV or .DAT 12869
A2890013.CSV or .DAT 180
A2890330.CSV or .DAT 16962
A3000200.CSV or .DAT 15941
A3000300.CSV or .DAT 11333 & 11334

It was also discovered during the quality control process that a cold bias existed in the virtual air temperature measured by the ATI sonic anemometer. The ATI reported temperatures on average about 5.5°C below that reported by the GILL sonic anemometer. The response was observed to be a linear function of temperature with the error becoming less at higher temperatures. The ATI sonic anemometer temperatures were adjusted according to that relationship.

Summary Statistics

Summary statistics were generated from the .RAW data files and placed in three other types of data files called .NRT, .FLX, and .ERR files. The naming convention of these files was *XXYY_DDD.ZZZ* where *XX=AT* for ATI or *XX=GI* for Gill, *YY=00* for year 2000, *DDD* is the day of year, and *ZZZ=NRT, FLX, or ERR*, and was derived from the names of the .CSV and .DAT data files. Summary statistics were not calculated for files containing less than 10 min of data, i.e., A2810530, G2810530, A2920530, G2920530, A3000600, and G3000600.

NRT data files, or non-rotated data files, contain summary statistics from data obtained directly from the sonic anemometers. Data included in the .NRT files were as follows:

1. Day of year
2. Time of first data point, obtained from the data file name (HHMM, MDT)
3. Wind direction (deg)
4. Average *w* (vertical) component wind speed (m s^{-1})
5. Average *u* (horizontal) component wind speed (m s^{-1})
6. Average *v* (horizontal) component wind speed (m s^{-1})
7. Average virtual air temperature ($^{\circ}\text{C}$)
8. Variance of the *w* wind component (m s^{-1})
9. Variance of the *u* wind component (m s^{-1})
10. Variance of the *v* wind component (m s^{-1})
11. Variance of virtual air temperature ($^{\circ}\text{C}$)
12. Covariance of *u* and *w* ($\text{m}^2 \text{s}^{-2}$)
13. Covariance of *u* and *v* ($\text{m}^2 \text{s}^{-2}$)
14. Covariance of *v* and *w* ($\text{m}^2 \text{s}^{-2}$)
15. Covariance of *w* and virtual air temperature ($^{\circ}\text{C m s}^{-1}$)
16. Covariance of *u* and virtual air temperature ($^{\circ}\text{C m s}^{-1}$)
17. Covariance of *v* and virtual air temperature ($^{\circ}\text{C m s}^{-1}$)
18. Total number of data points in the file

The data in the .FLX files were subjected to a two-dimensional coordinate rotation. It is from these files that 30-min values of momentum flux and heat flux can be calculated. The coordinate rotation comprised a horizontal rotation about the vertical axis and a vertical rotation about the *v*-component axis. The resulting 30-min average value of *u* is the wind speed. The vertical rotation was undertaken to minimize the 30-min average of *w*, since it is assumed that the sonic anemometers were not installed in a truly level condition. The data included in the .FLX files were as follows:

1. Day of year
2. Time of first data point, obtained from the data file name (HHMM, MDT)
3. Wind direction (deg)
4. Average wind speed (m s^{-1})
5. Covariance of rotated *u* and *w* ($\text{m}^2 \text{s}^{-2}$)
6. Average virtual air temperature ($^{\circ}\text{C}$)

7. Variance of the rotated u wind component (m s^{-1})
8. Variance of the rotated v wind component (m s^{-1})
9. Variance of the rotated w wind component (m s^{-1})
10. Variance of the virtual air temperature ($^{\circ}\text{C}$)
11. Covariance of rotated w and virtual air temperature, i.e., kinematic sensible heat flux ($^{\circ}\text{C m s}^{-1}$)
12. Rotation angle about the y axis (deg)
13. Rotation angle about the z axis (deg)
14. Total number of data points in the file

Item 11 above (the covariance of the rotated w wind component and virtual air temperature) can also be expressed as $\overline{w'T'_v}$. When represented in this manner, it is of the same form as kinematic sensible heat flux ($\overline{w'T'}$), where T is dry bulb temperature. T can be easily obtained from T_v if atmospheric humidity is known. The humidity values from the FRD surface meteorology site (see next chapter) are probably sufficiently accurate for this purpose. Actual sensible heat flux (H) can then be calculated from the kinematic sensible heat flux if air density (ρ_a) can also be determined (Stull, 1988). The appropriate equation is:

$$H = \rho_a C_p \overline{w'T'} \quad (1)$$

where C_p is the specific heat of air at constant pressure ($1004 \text{ J kg}^{-1} \text{ K}^{-1}$). H has units of W m^{-2} .

Item 5 above (the covariance of the rotated w wind component and the rotated u wind component) is known as kinematic momentum flux and can be written as $\overline{u'w'}$. Actual momentum flux (τ) can be calculated if air density is known as follows:

$$\tau = \rho_a \overline{u'w'} \quad (2)$$

and has units of $\text{kg m}^{-1} \text{ s}^{-2}$. The square root of the absolute value of $\overline{u'w'}$ is known as friction velocity (u_*), with units of m s^{-1} (Stull, 1988). Friction velocity is a measure of the strength of shear-generated turbulence.

The .ERR data files contain statistical summaries that are used primarily for quality control. The data included in these files were as follows:

1. Day of year
2. Time of first data point, obtained from the data file name (HHMM, MDT)
3. Wind direction (deg)
4. Skewness of w wind component
5. Skewness of u wind component
6. Skewness of v wind component

7. Skewness of virtual air temperature
8. Kurtosis of w wind component
9. Kurtosis of u wind component
10. Kurtosis of v wind component
11. Kurtosis of virtual air temperature
12. Total number of data points in the file

Sonic Anemometer Comparison

Analysis of the summary statistics indicates very little difference in performance between the two sonic anemometers, even though they were separated vertically by nearly 3 m. Table 2 lists averages and variances of parameters included in the .FLX files. Essentially no difference in wind speed, wind direction, or the variances of the various wind components was observed. The average virtual temperature measured by the two anemometers was identical because of the adjustment made to the ATI temperature data mentioned above. The variance in the GILL virtual air temperature was 57% higher than that of the ATI.

Table 2 shows that the average wind speed for all 7 IOPs was very light at 0.6 m s^{-1} . The vector average wind direction was 113 deg, indicating the wind was generally from the east-southeast. These two parameters were probably largely influenced by the nearby City Centre building located to the south and east (upwind) of the sonic installation.

Kinematic heat flux measured by the two anemometers was also quite different, although very small in magnitude. The ATI measured heat flux values were 84% larger than the GILL. However, assuming a combined air density and specific heat value of $1000 \text{ J m}^{-3} \text{ }^{\circ}\text{C}^{-1}$ (an approximate value for Salt Lake City), the resulting heat flux would only be about -3 W m^{-2} . The negative sign indicates a slight downward heat flux from the air to the surface.

Table 2. Average and variance of the parameters included in the .FLX files for the ATI and GILL sonic anemometers.

Variable	Units	ATI Sonic Anemometer	GILL Sonic Anemometer
Average wind speed	m s^{-1}	0.63	0.62
Vector average wind direction	deg	113.4	113.4
Average virtual temperature	$^{\circ}\text{C}$	16.64	16.64
Variance of rotated u component	m s^{-1}	0.228	0.236
Variance of rotated v component	m s^{-1}	0.217	0.223
Variance of rotated w component	m s^{-1}	0.0724	0.0544
Variance of virtual air temperature	$^{\circ}\text{C}$	0.0457	0.0717
Average kinematic momentum flux	$\text{m}^{-2} \text{s}^{-2}$	0.131	0.132
Average friction velocity	m s^{-1}	0.362	0.363
Average kinematic sensible heat flux	$^{\circ}\text{C m s}^{-1}$	-0.00297	-0.00161

UPPER-AIR AND STANDARD SURFACE METEOROLOGY STATION

A 10-m tower (Fig. 5) with standard meteorological instrumentation, a phased-array Doppler sodar, and a radar wind profiler (Fig. 6) acquired surface and upper-air meteorological data during the URBAN 2000/VTMX field study. These instruments were deployed over a three-week period in a open dirt parking lot on the grounds of the Raging Waters entertainment complex located at 1200 West 1700 South, Salt Lake City (40° 43.92' N, 111° 55.65' W, elevation 1291 m MSL). This site was approximately 5 km southwest of downtown Salt Lake City. The Raging Waters location is shown relative to the downtown location and the entire Salt Lake Valley in Fig. 7.

Urban locations are usually not well suited for siting meteorological towers and remote sensors because of the close proximity of buildings and other obstructions. However, the Raging Waters complex was a remarkably idle site for surface and upper-air meteorological monitoring with few obstructions. The tower and remote sensors were located on the southern end of a large dirt parking lot. Residential homes were located about 500 m on the north side of the



Figure 5. Meteorological tower and associated instrumentation.



Figure 6. Doppler sodar and radar wind profiler.

east-west running street (West 1700 South). To the south of this measurement site was the northern border of Glendale Golf Course. To the west were a few trees and a public park. The only major obstructions were the water slides about 200 m to the east which were about 15 to 25 m in height.

A set of vista photographs of the Raging Waters complex was taken towards the eight cardinal compass points. The left and right photographs of the first row in Fig. 8 are views to the north and northeast, respectively. The photos in the second row are views to



Figure 8. Raging Waters vista photos.

10-m Tower

A 10-m open-lattice aluminum tower purchased from Universal Manufacturing was deployed in the dirt parking lot. A Climatronics F460 cup anemometer and vane were used to measure wind speed and wind direction, respectively, at 10 m above the ground. A Vaisala HMP-45AC probe housed inside an R. M. Young multi-plate radiation shield provided air temperature and relative humidity at 2 m. These sensors were sampled once per second and averaged over 5-min intervals by a Campbell Scientific CR-10 data logger. Electrical power needed to run the sensors and data logger was supplied by a rechargeable battery and a 10-W solar panel. The data logger time was set to Mountain Daylight Saving Time (MDT). A total of 6794 records was recorded between 1910 MDT on October 3, 2000 and 0915 MDT on October 27, 2000. These sensors were thoroughly tested and calibrated before deployment using U. S. EPA (1995, 2000) guidelines and procedures.

A wind rose of this tower-based data for the three-week deployment period shows a predominately southeasterly wind flow generally ranging from 1 to 4 m s⁻¹ (Fig. 9). A second maximum of 2 to 4 m s⁻¹ from the northwest suggests a lake breeze flow which was typically observed in the late afternoon. For the most part, wind speeds were generally less than 5 m s⁻¹ during the study with very light winds (< 2 m s⁻¹) observed during the evening and early morning hours. Weekly time series plots of the vector wind speed, vector wind direction, standard deviation of the wind direction (σ_{θ}), air temperature, relative humidity, and data logger battery voltage (provided for quality control) are shown in Figs. 10-13.

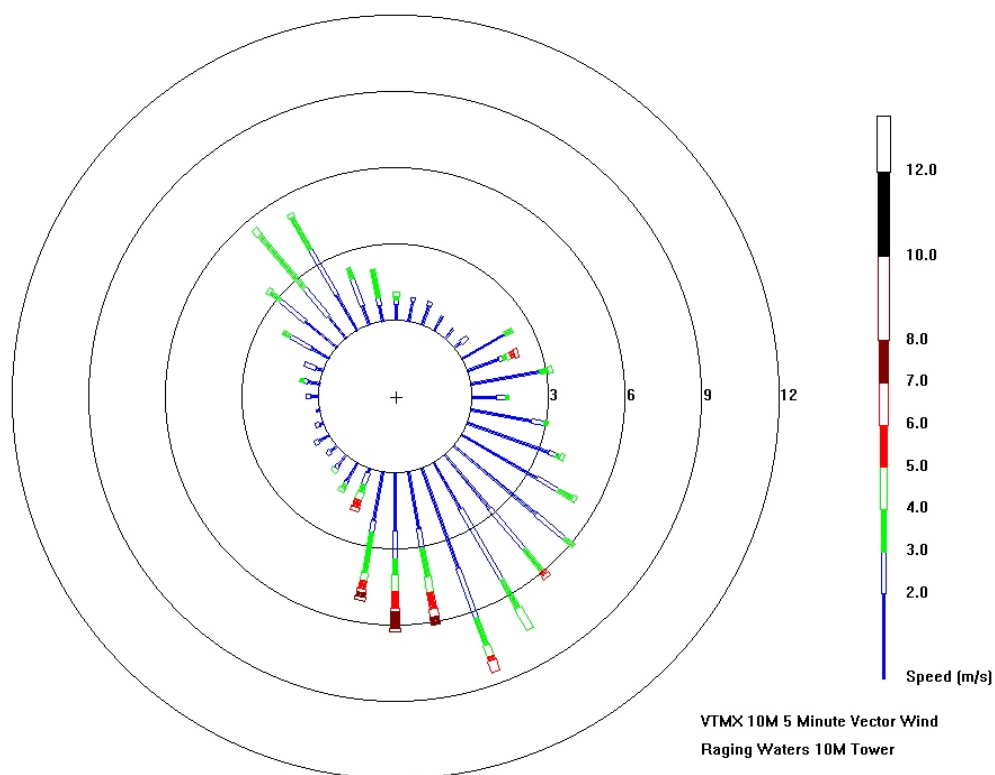


Figure 9. Wind rose for 10-m tower.

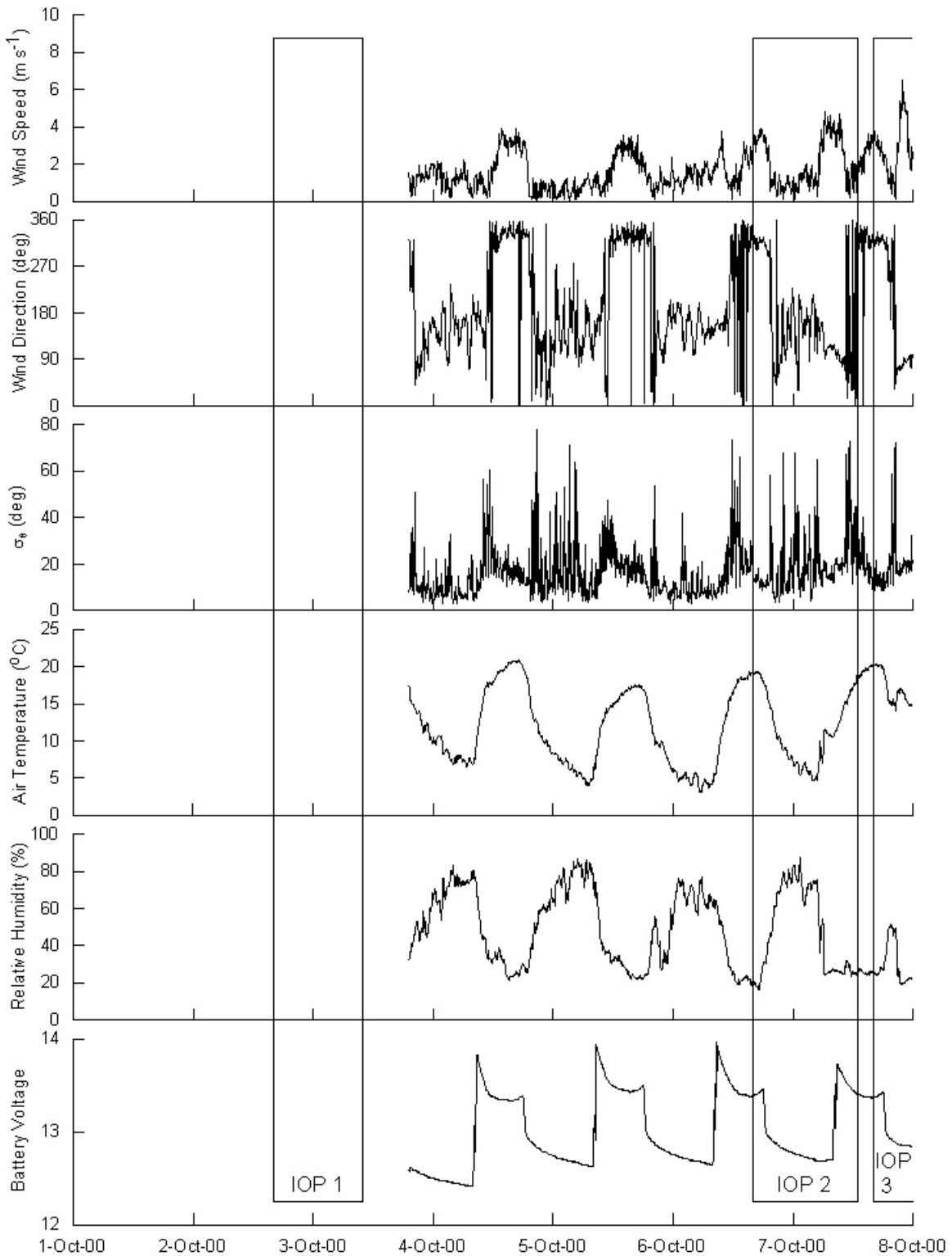


Figure 10. Time series of tower-based vector wind speed, vector wind direction, standard deviation of the wind direction (σ_θ), air temperature, relative humidity, and battery voltage from October 1-8, 2000.

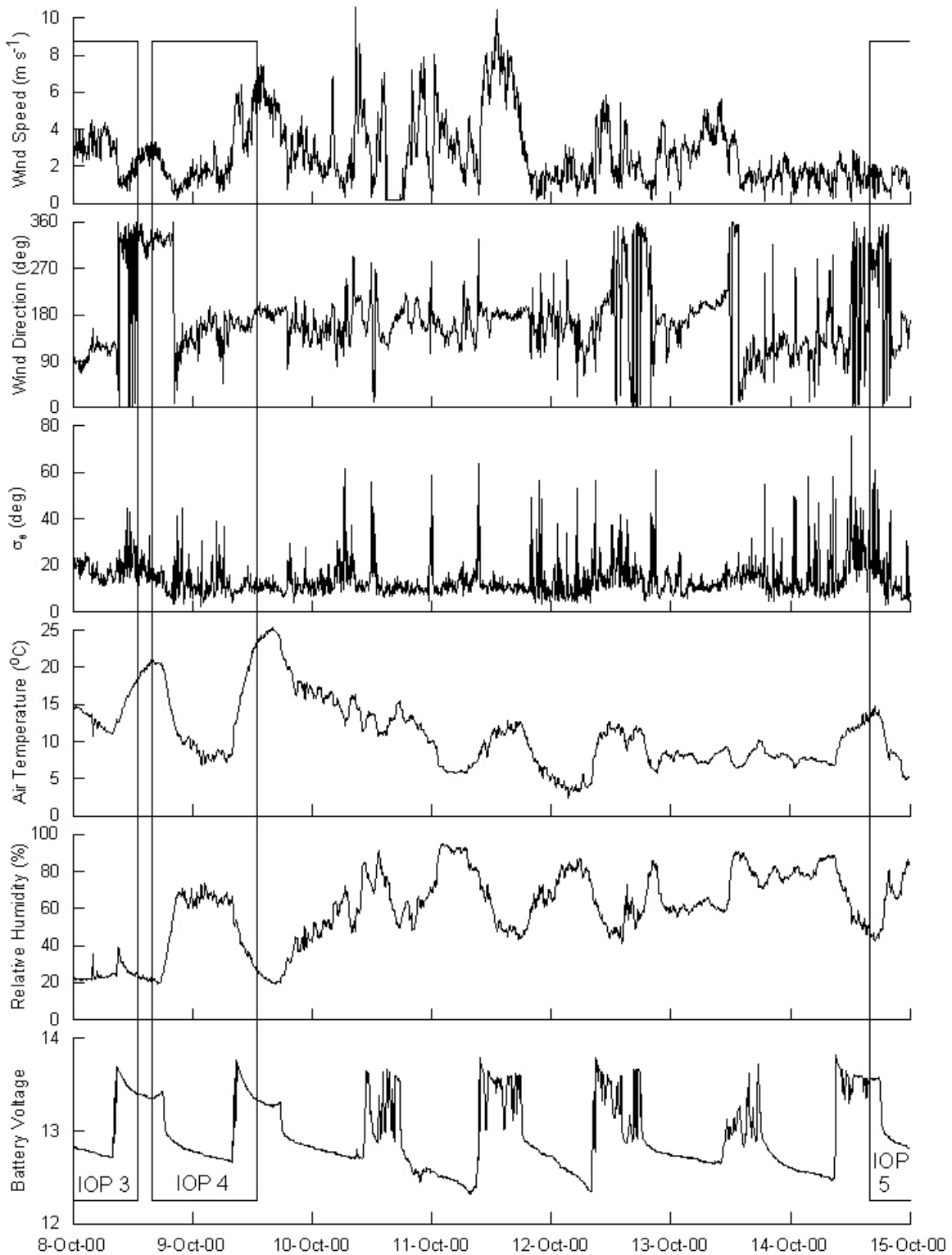


Figure 11. Time series of tower-based vector wind speed, vector wind direction, standard deviation of the wind direction (σ_{θ}), air temperature, relative humidity, and battery voltage from October 8-15, 2000.

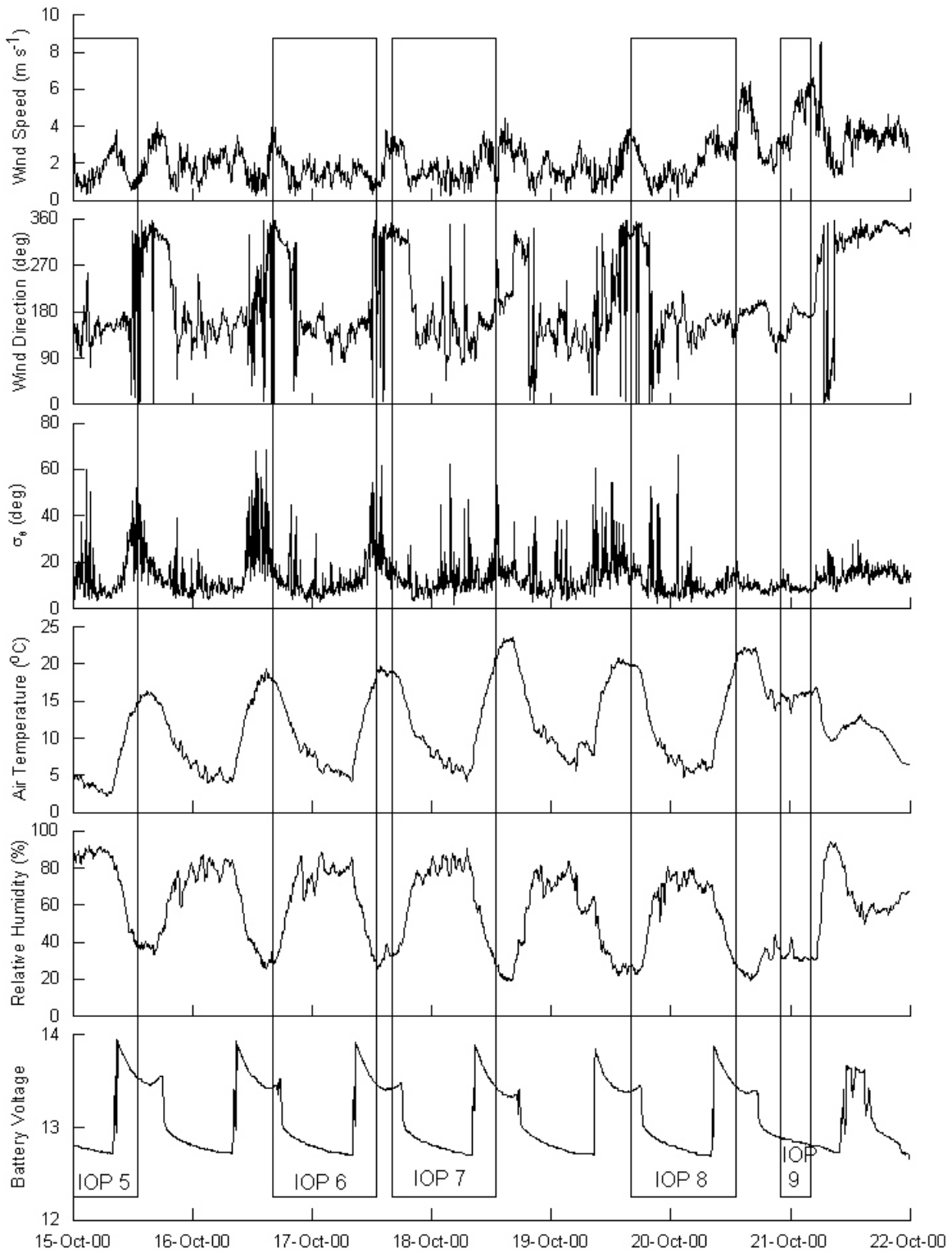


Figure 12. Time series of tower-based vector wind speed, vector wind direction, standard deviation of the wind direction (σ_θ), air temperature, relative humidity, and battery voltage from October 15-22, 2000.

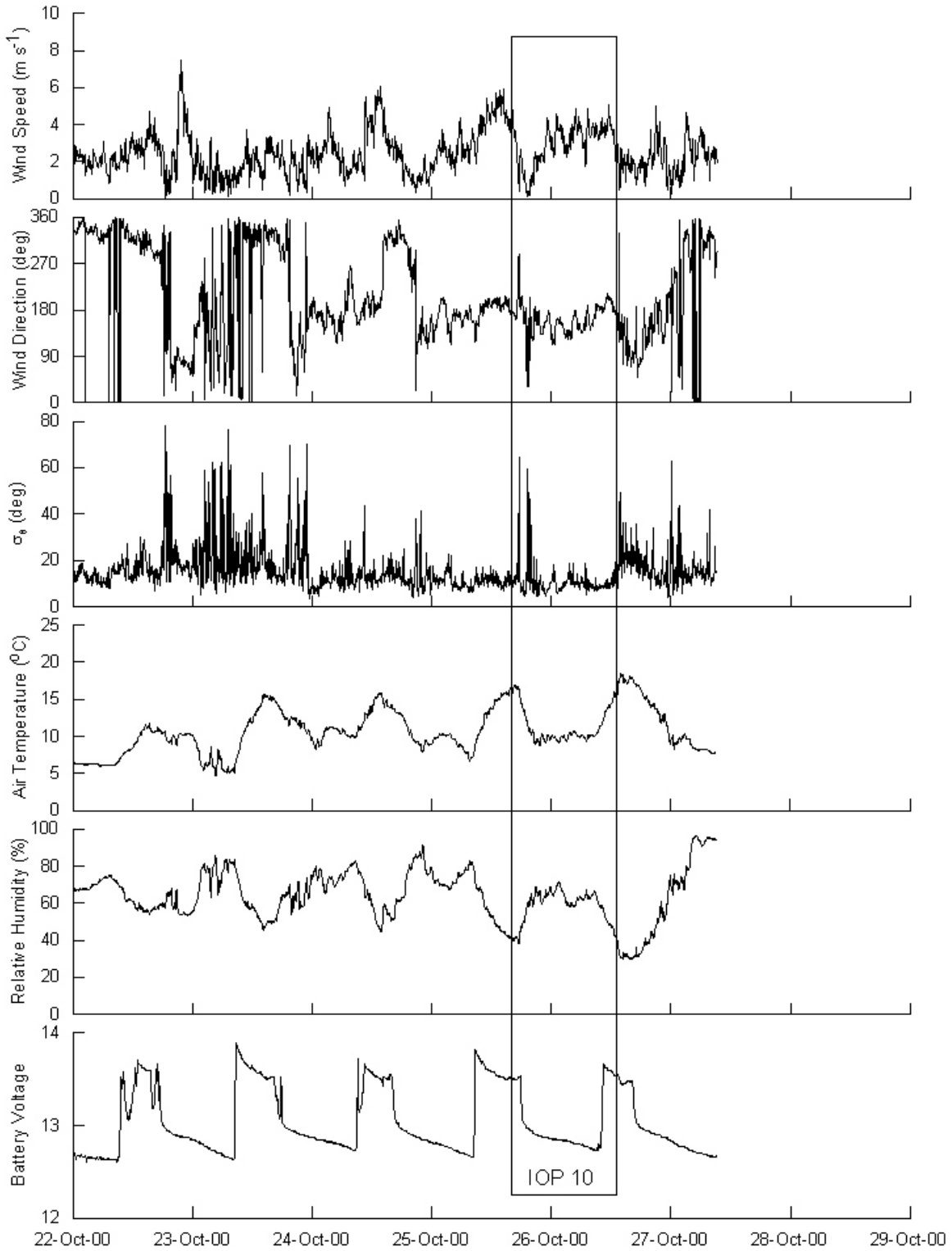


Figure 13. Time series of tower-based vector wind speed, vector wind direction, standard deviation of the wind direction (σ_{θ}), air temperature, relative humidity, and battery voltage from October 22-29, 2000.

Sodar and Radar

A Radian 600PA phased-array Doppler sodar was used to acquire wind profiles in the first 300 m of the atmospheric boundary layer. Wind profiles were acquired between 1330 MDT on October 4, 2000 and 0915 MDT on October 27, 2000. The data acquisition computer time was set to MDT. The sodar was configured to acquire 15-min wind profiles from 40 to 300 m with a 10-m resolution. The output frequency of the sodar was increased to ~3 KHz in order to avoid ambient noise contamination of the wind profile data (Crescenti 1998; Crescenti and Baxter 1998).

A Radian 915-MHz phased-array radar wind profiler was used to acquire wind profiles up to a height of about 3 km. Wind profiles were acquired between 1400 MDT on October 4, 2000 and 0800 MDT on October 27, 2000. The data acquisition computer time was also set to MDT. The radar was configured to acquire one-hour wind profiles in a dual mode. The first mode acquired high-resolution, low-range data from 124 to 2158 m with a resolution of about 55 m. The second sampling mode acquired low-resolution, high-range data from 172 to 3732 m with a resolution of about 96 m.

The along-axis of the flat-bed trailer that carried the sodar and radar antennas was oriented along 15° and 195° with respect to true north. The trailer and antennas were leveled to within $\pm 0.2^\circ$ in accordance with U. S. EPA guidance and procedures (1995, 2000). The two oblique-angle (14.87° from the vertical) acoustic sodar beams which are used to derive the horizontal wind components (U and V) were oriented to the south-southwest (195°) and west-northwest (285°), respectively. A diagnostic test was executed on the sodar during the installation process to identify any faulty acoustic transducers. Eight out of 120 acoustic transducers did not function properly (Fig. 14). Broken signal lines between the data acquisition system and the antenna are responsible for the individual transducer malfunctions. However, the phased-array sodar can still acquire reliable data even if 10% of the transducers do not function (assuming they are randomly distributed). The radar antenna was extensively tested and was found to operate within normal parameters. The four oblique-angle radar beams which are used to derive the horizontal wind components were oriented to the north-northeast (15°), east-southeast (105°), south-southwest (195°), and west-northwest (285°). Software acquisition versions for the sodar and radar were 3.0.33 and POP4.x, respectively.

Upper-air data were passed through quality control screening algorithms that objectively removed questionable data such as spikes and outliers (Weber and Wuertz 1991; Weber et al. 1993). Afterward, upper-air climatological plots of the sodar data were generated based on the methodology developed by Wilczak et al. (1997). Figure 15 is a contour plot of data availability (i.e., the percentage of valid data reported by the sodar). In general, the percentage of valid data acquired by the sodar was very high. At least 50% of the data were reported for the entire sampling range of the sodar from prior to midnight to about 1300 MDT. The sodar range became more limited during the afternoon to early evening with the 50% data availability level dropping down to about 250 m.

Analysis of the average scalar wind speeds from the sodar indicate that the strongest winds (with respect to magnitude) occur from late evening (~ 2200 MDT) to early morning (~ 0900 MDT) above 150 m with a scalar wind speed of 5 to 7 m s^{-1} (Fig. 16). The weakest winds tend to occur

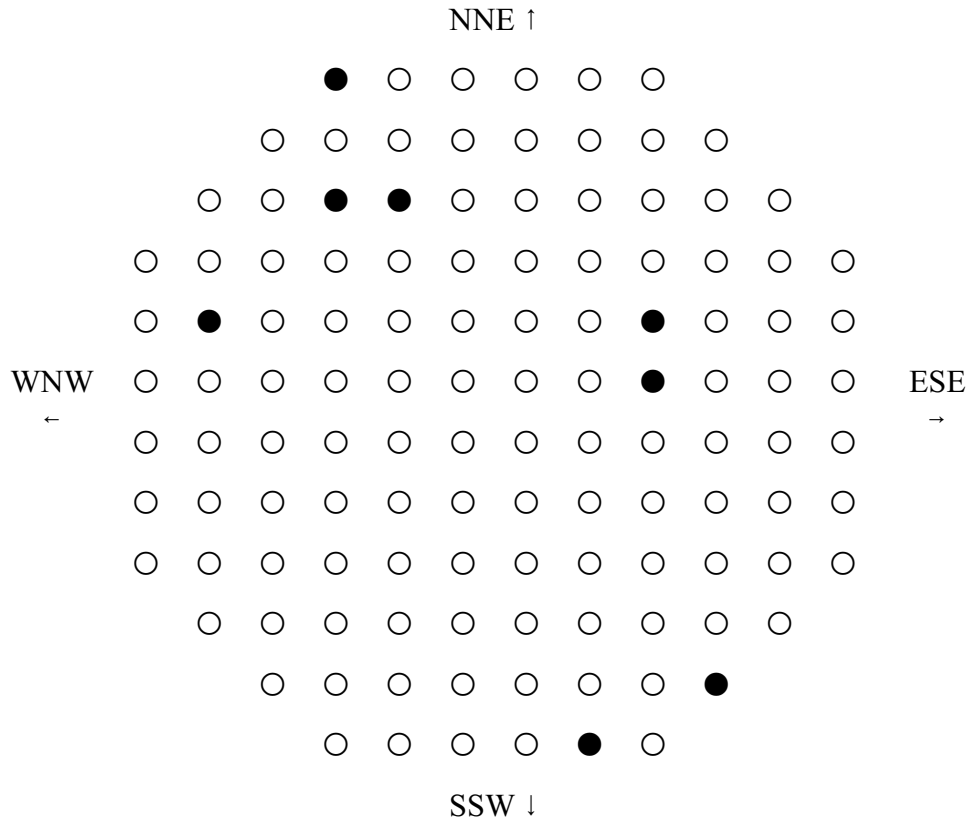


Figure 14. Representation of the 120-transducer phased-array Doppler sodar antenna. Functional transducers are depicted by ○ while nonfunctional transducers are depicted by ●.

from late morning to early afternoon (1000 to 1400 MDT) and in the early evening (1800 to 2100 MDT) with scalar wind speeds averaging less than 3 m s^{-1} from near the surface up through 300 m.

Contours of vector average wind speed are shown in Fig. 17. Over the three-week period, a fairly persistent southeasterly wind of 3 to 4 m s^{-1} was observed by the sodar from the surface up to 300 m in the early morning hours prior to sunrise. A couple of hours after sunrise, the mean wind speed decreases to about 1 to 2 m s^{-1} and veers with time to a southerly flow by late morning and to a southwesterly flow by early afternoon. As the day progresses, the winds continue to veer. A shallow northwesterly flow exists in the late afternoon to a height of about 80 to 90 m. These data suggest that this flow may be a weak lake breeze. Above 100 m in the late afternoon, the winds tend to be more westerly and less persistent. Winds tend to be very light and variable through 300 m for a couple of hours after sunset. However, the wind speeds quickly strengthen and become more organized out of the southeast after 2100 MDT. In fact, the data suggest the formation of a 5 m s^{-1} southeasterly jet between 250 and 300 m between 2200 MDT and midnight.

Figure 18 is a contour plot of the persistence of the wind. Persistence is simply the ratio of the vector wind speed to the scalar wind speed. A value near 100% would represent a “persistent”

wind that varies little over this three-week average while a low value represents a random wind flow pattern. The most persistent flow is the southeasterly winds in the late evening through early morning hours while the least persistence winds tend to occur in the afternoon and early evening hours.

Figures 19 and 20 show the average radar data availability as a function of time and height. In general, the available data decreases with height in both modes and is relatively indifferent to the time of day. Figures 21 and 22 are scalar wind speed plots for both radar modes. The strongest winds tend to occur in the predawn hours with a maximum of near 10 m s^{-1} at about 2000 m. The winds tend to relax in the afternoon at the lower levels of the atmospheric boundary layer. Contours of vector average wind speed are shown in the time/height plots in Figures 23 and 24. The radar data suggest that the lake breeze is approximately 400 m deep and is observed at Raging Waters for no more than a couple of hours. From 500 to 1000 m, the mean flow is predominately from the south for the entire day. The flow becomes more southwesterly and westerly above 1200 m. Missing data are found at the higher range gates because of the lack of sufficient turbulence to scatter the transmitted signal back to the radar. Winds from 1800 to 3000 m also are predominately from the southwest throughout much of the day. Finally, persistence plots are shown in Figures 25 and 26. As in the case of the sodar data, the radar winds are the most persistence in the early morning hours with a southerly flow and least persistent in the afternoon when the weak lake breeze is sometimes observed.

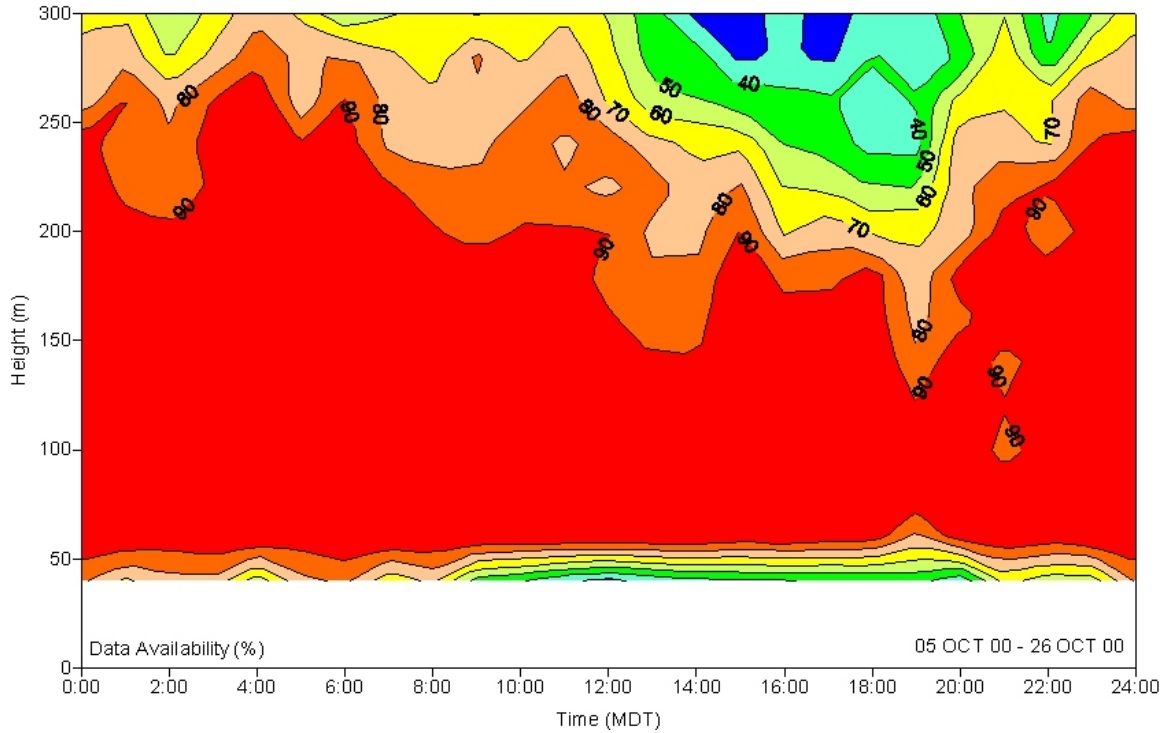


Figure 15. Sodar data availability as a function of time and height.

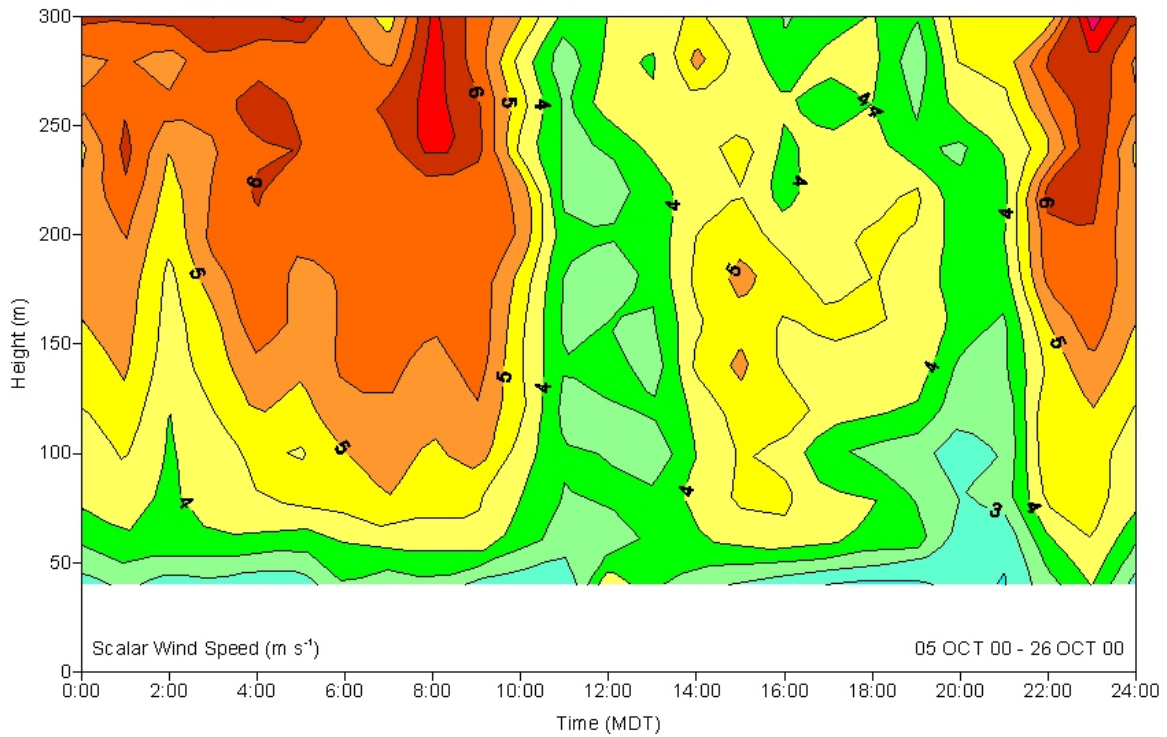


Figure 16. Average sodar scalar wind speed as a function of time and height.

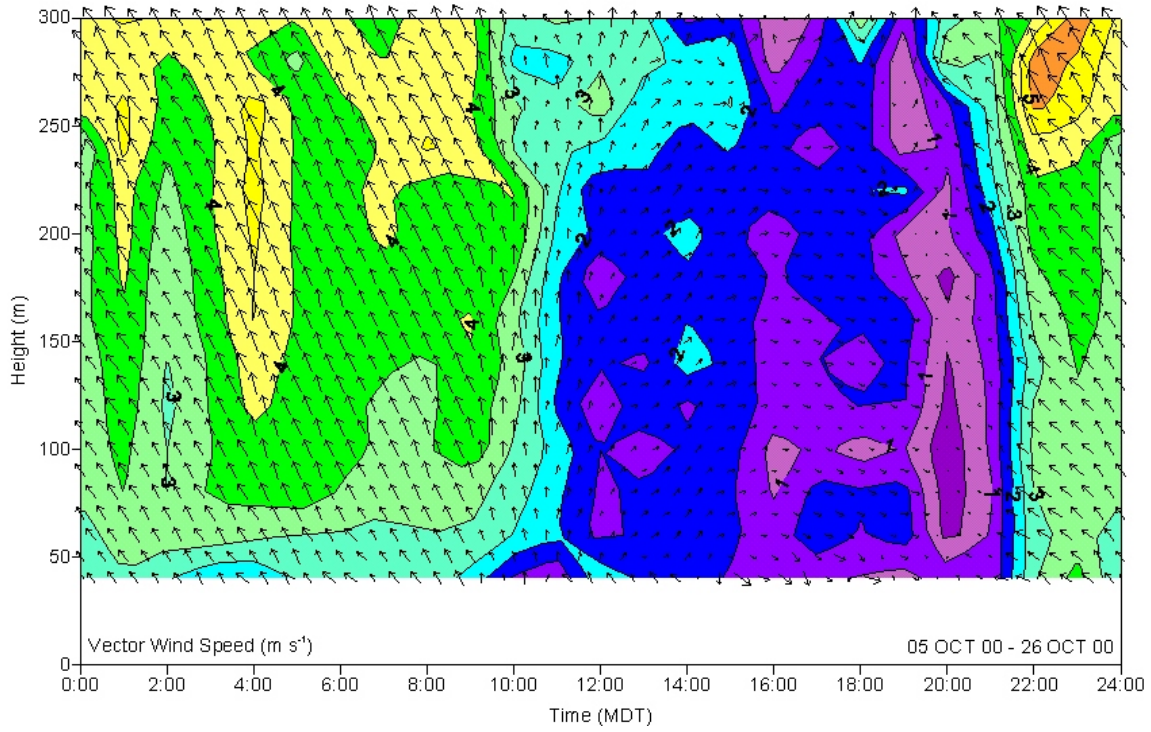


Figure 17. Sodar vector wind speed as a function of time and height.

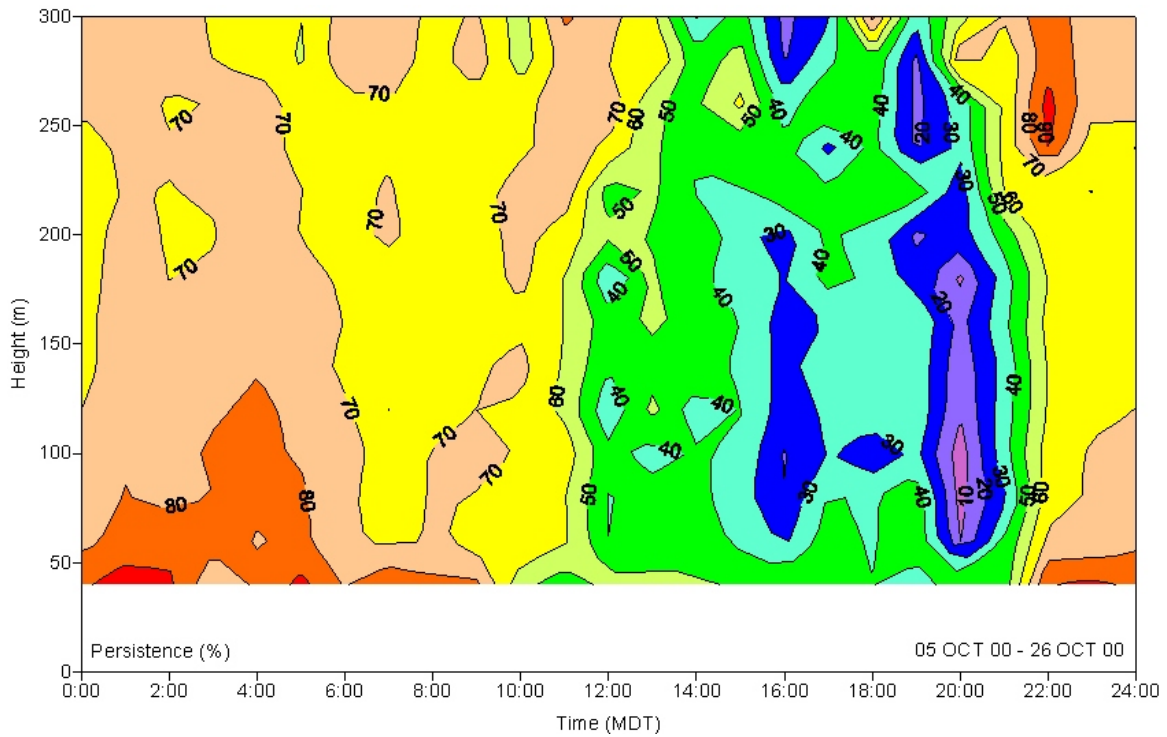


Figure 18. Sodar wind persistence as a function of time and height.

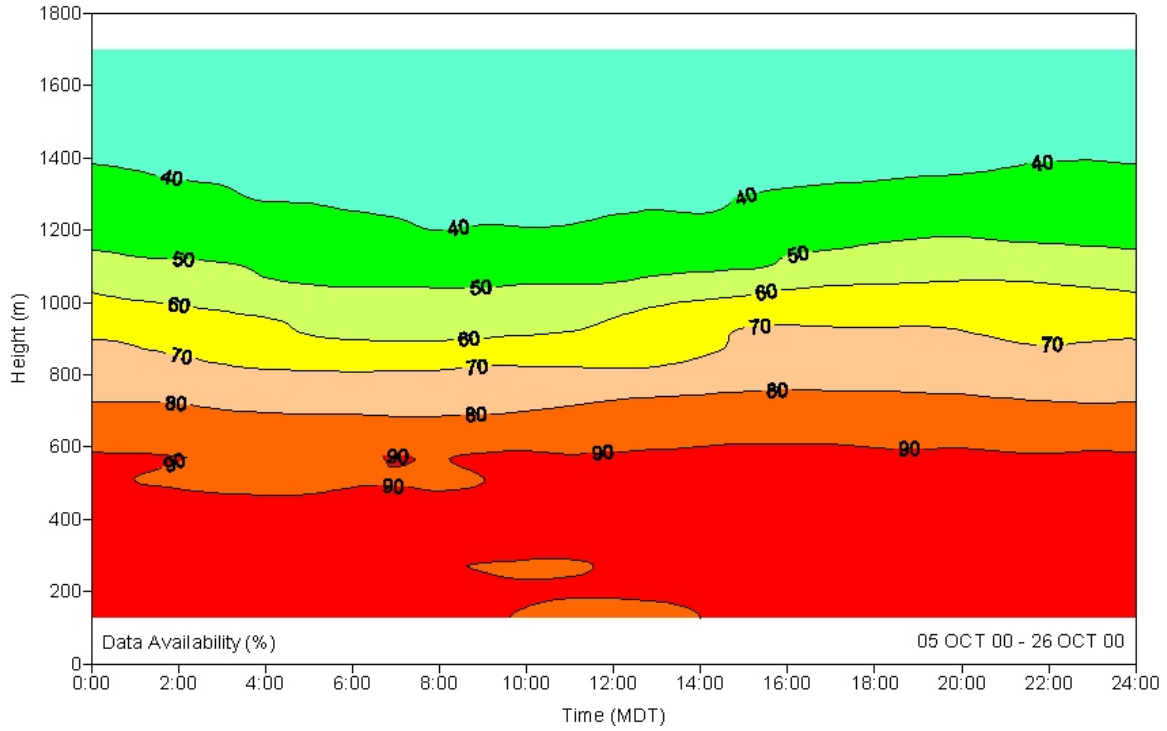


Figure 19. Radar (mode 1) data availability as a function of time and height.

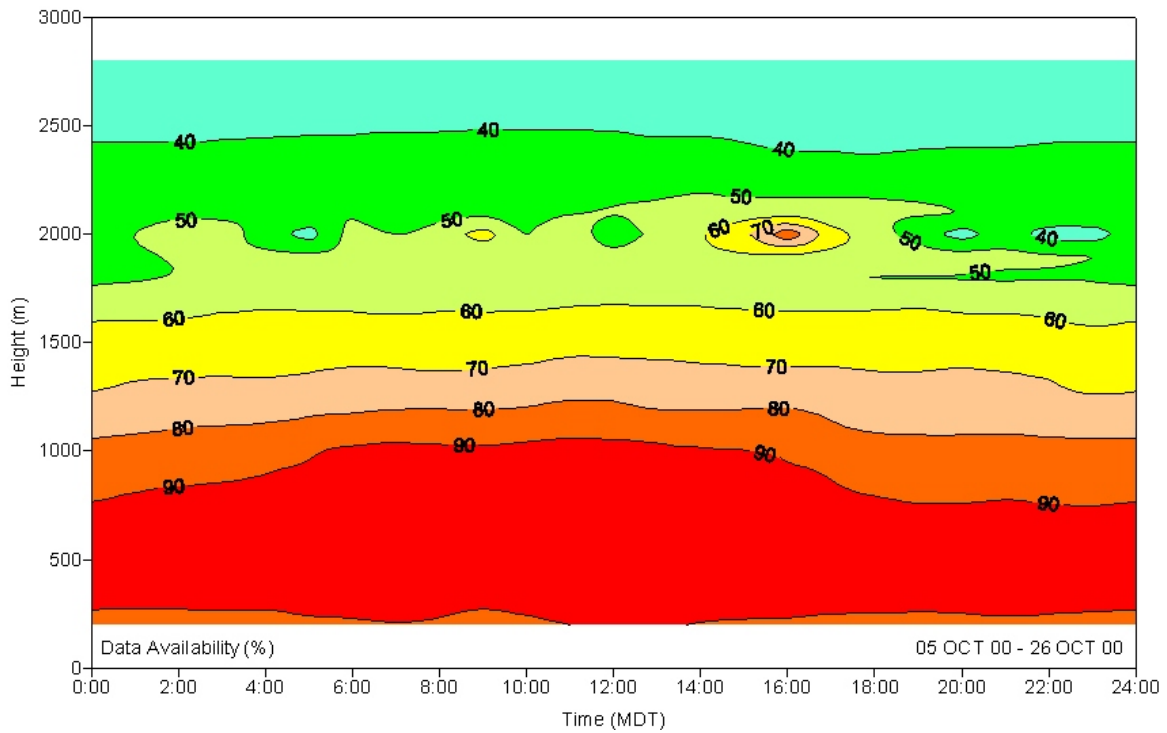


Figure 20. Radar (mode 2) data availability as a function of time and height.

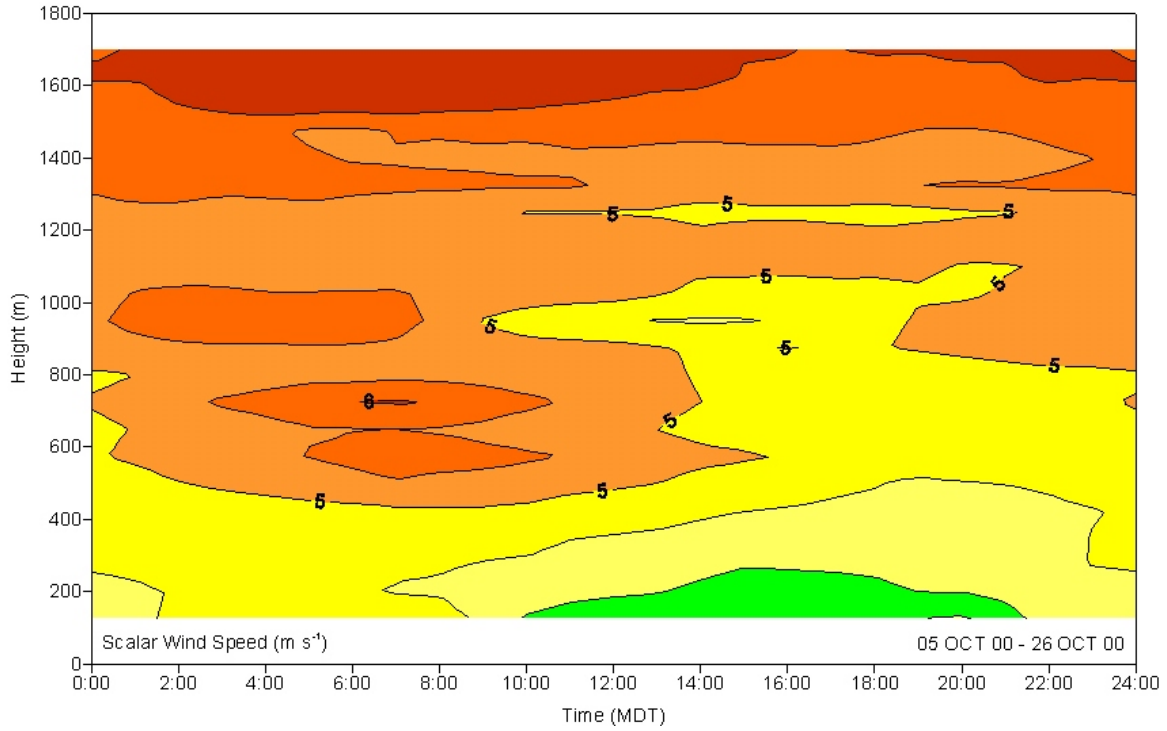


Figure 21. Radar (mode 1) scalar wind speed as a function of time and height.

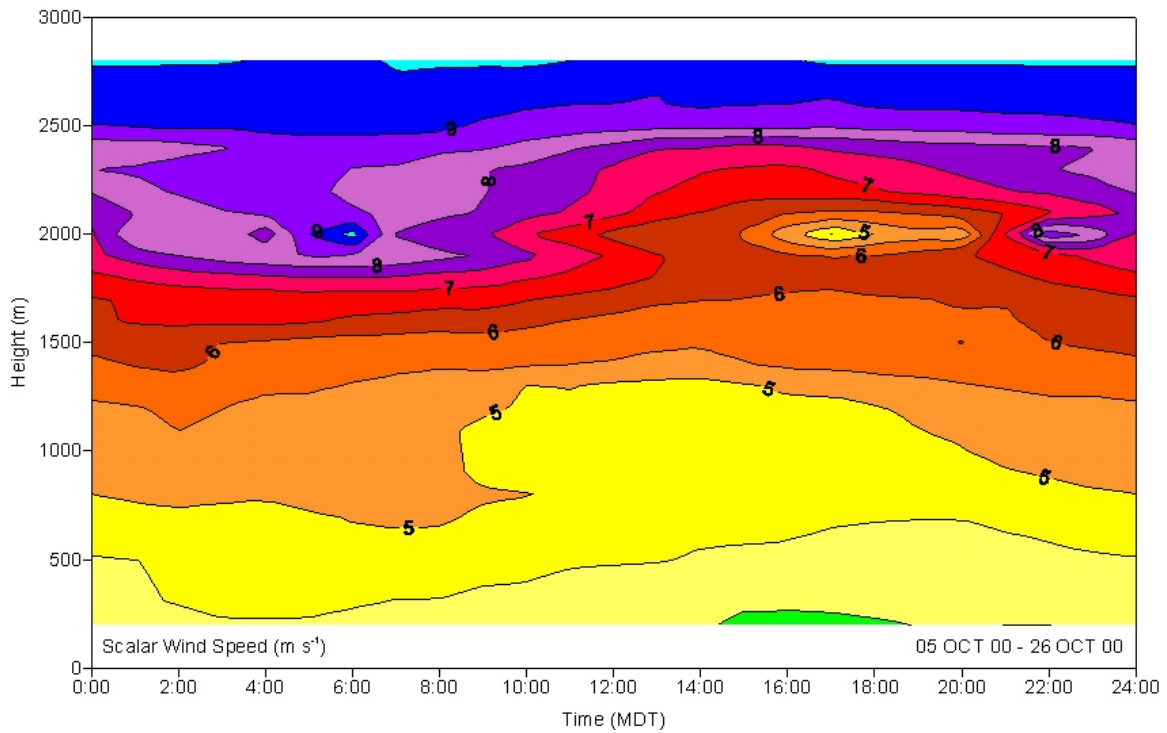


Figure 22. Radar (mode 2) scalar wind speed as a function of time and height.

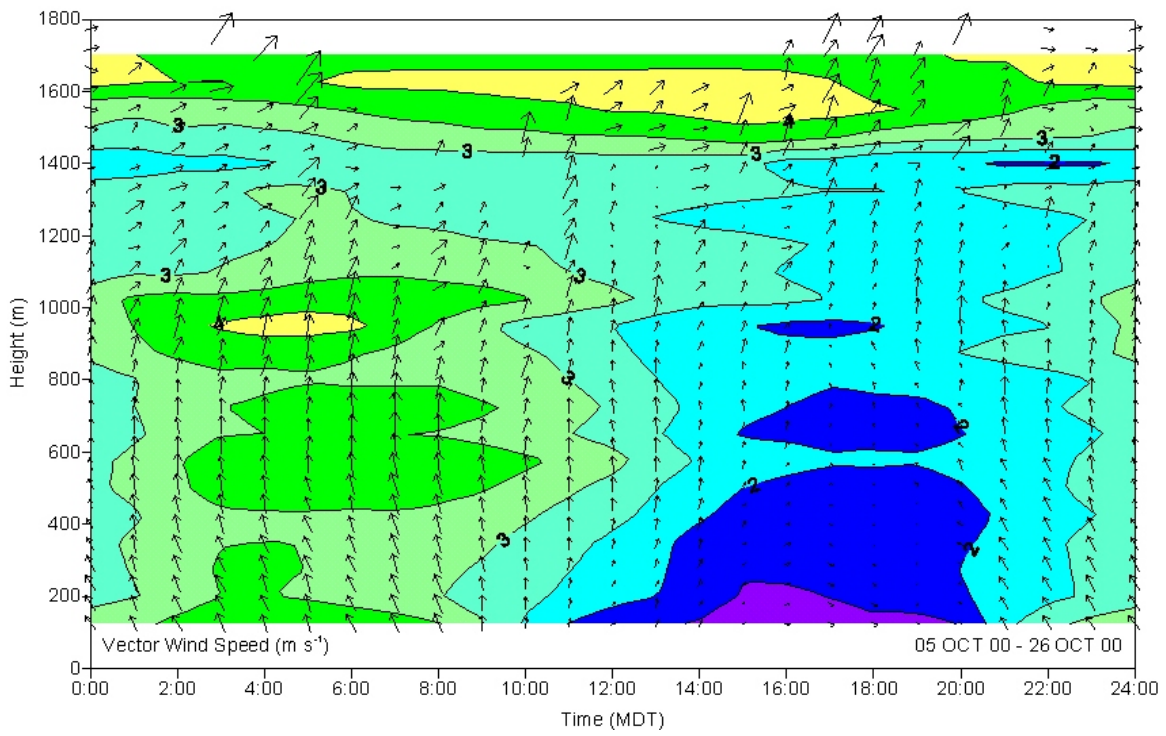


Figure 23. Radar (mode 1) vector wind speed as a function of time and height.

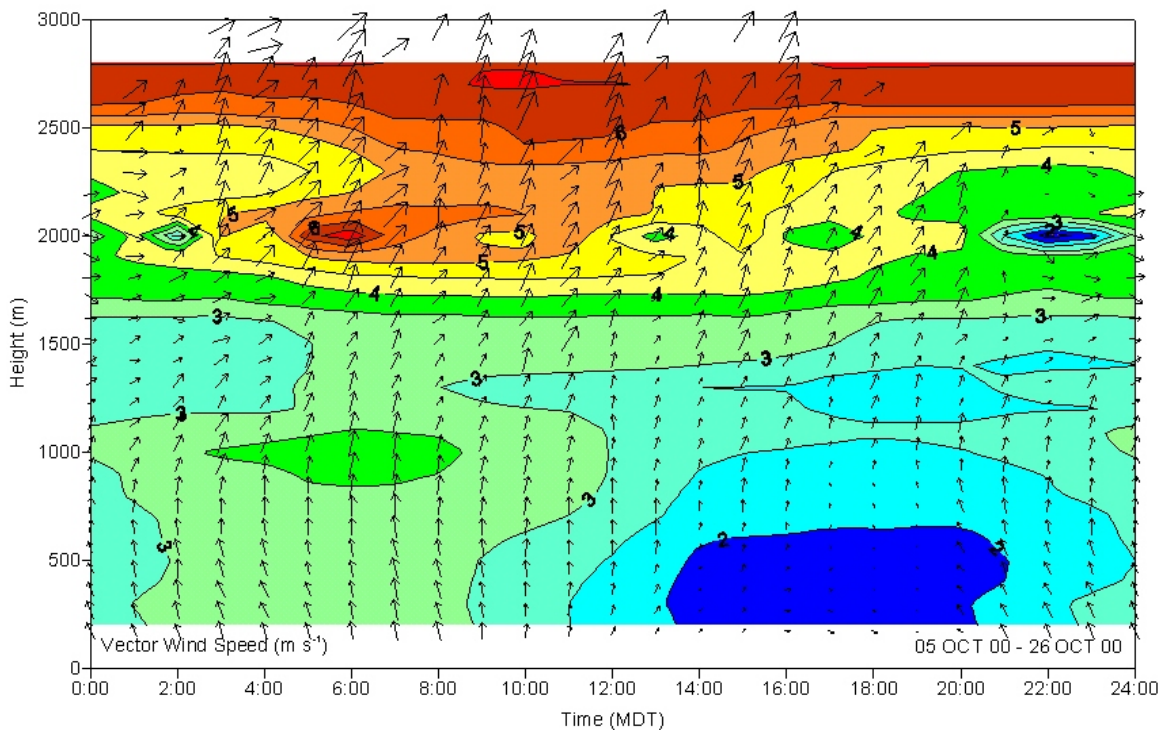


Figure 24. Radar (mode 2) vector wind speed as a function of time and height.

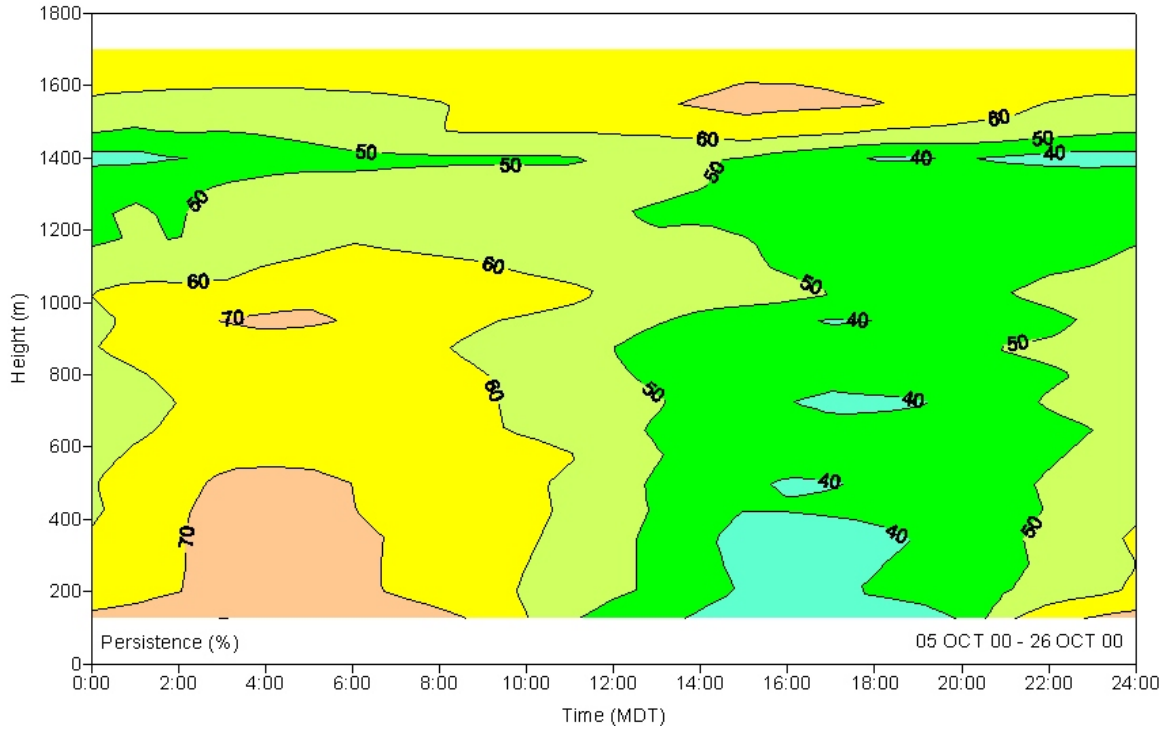


Figure 25. Radar (mode 1) wind persistence as a function of time and height.

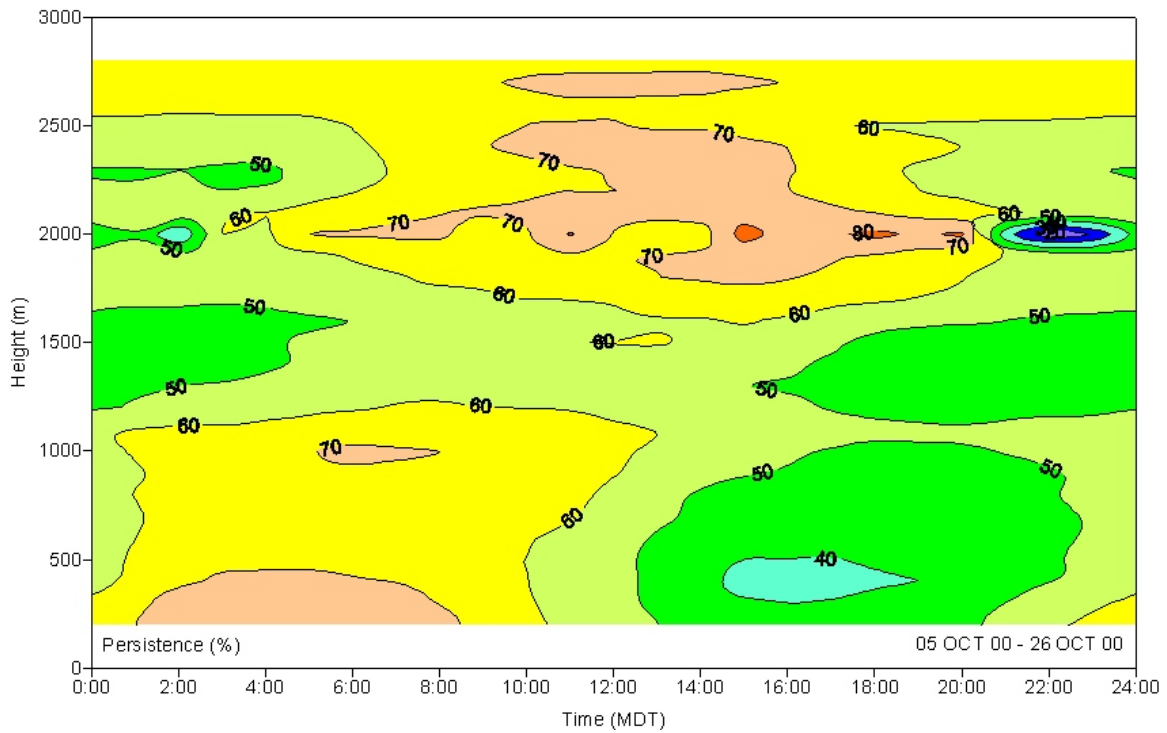


Figure 26. Radar (mode 2) wind persistence as a function of time and height.

This Page Intentionally Blank

INTENSIVE OBSERVATION PERIOD (IOP) CASE STUDIES

Eight out of ten URBAN 2000/VTMX intensive observation periods (IOPs) included an atmospheric tracer release component. During these IOPs, atmospheric tracers were released primarily in support of URBAN 2000. These IOPs, together with the associated time period of study, time of atmospheric SF₆ tracer release, and summary meteorological observations are given in Table 3. The information in this table is based on that from Allwine et al. (2002).

Table 3. Summary of URBAN 2000/VTMX IOPs.

IOP	IOP Start		Tracer Start		Tracer End		IOP End		Meteorological Summary
	Date	Time MDT	Date	Time MDT	Date	Time MDT	Date	Time MDT	
1	02 OCT	1600	03 OCT	0100	03 OCT	0400	03 OCT	0500	Clear skies, weak winds, well-developed drainage
2	06 OCT	1600	07 OCT	0100	07 OCT	0700	07 OCT	1300	Strong easterly down-slope winds after 0000-0300 MDT penetrating 1-2 km into valley
3	07 OCT	1600					08 OCT	1300	High winds
4	08 OCT	1600	09 OCT	0100	09 OCT	0700	09 OCT	1300	Clear skies, weak winds, well-developed drainage, approaching trough
5	14 OCT	1600	15 OCT	0100	15 OCT	0700	15 OCT	1300	Clear skies, weak winds, well-developed drainage
6	16 OCT	1600					17 OCT	1300	Clear skies, weak winds, well-developed drainage
7	17 OCT	1600	18 OCT	0100	18 OCT	0700	18 OCT	1300	Clear skies, weak winds, well-developed drainage, approaching trough
8	19 OCT	1600	20 OCT	0100	20 OCT	0700	20 OCT	1300	Clear skies, weak winds, well-developed drainage
9	20 OCT	2200	20 OCT	2200	21 OCT	0300	21 OCT	0400	Cloudy skies, weak to moderate winds, weak drainage, approaching trough
10	25 OCT	1600	26 OCT	0100	26 OCT	0700	26 OCT	1300	Cloudy skies, moderate winds, weak drainage, approaching trough

Data from the two sonic anemometers were acquired for seven of the eight atmospheric tracer IOPs and are summarized in Table 4. From the general meteorological observations, the sonic anemometer data could be grouped into three distinct categories. IOPs 2, 4, 5, 7, and 10 were quite similar in wind speed and wind direction. IOP 10 was grouped in this category even though an approaching trough affected the winds toward the end of the test period. IOP 1 was in a separate category primarily because of the wind direction. IOP 9 was also in a separate category because of the increased wind speed as well as a distinctly different wind direction.

Table 4. Sonic anemometer summary statistics for each IOP.

IOP	Wind Speed (m s ⁻¹)	Wind Direction (deg)	Virtual Temperature (°C)	Kinematic Momentum Flux (m ² s ⁻²)	Kinematic Sensible Heat Flux (°C m s ⁻¹)
1	0.53	169.9	20.1	0.13	0.0014
2	0.47	115.6	15.8	0.16	-0.0009
4	0.50	106.5	16.2	0.10	-0.0033
5	0.59	117.1	12.8	0.12	-0.0035
7	0.58	118.0	15.3	0.09	-0.0001
9	1.12	64.2	19.7	0.14	-0.0047
10	0.62	100.9	15.8	0.18	-0.0054
Average	0.63	113.4	16.6	0.13	-0.0023

Doran et al. (2002), however, defined two major meteorological categories of IOPs. Their analysis is quoted here in full for the benefit of the reader for easier understanding of the results that follow in this publication.

“IOPs with well-developed drainage circulations. IOPs 5 (14–15 October), 6 (16–17 October), and 8 (19–20 October) can be characterized by clear skies, weak winds aloft at crest level, strong nocturnal radiation inversions, limited moisture in the boundary layer, and pronounced drainage flow into the Salt Lake Valley from the west, south, and east. The surface-based inversions and drainage circulations developed after sunset and persisted without significant interruption until sunrise. While the synoptic and mesoscale conditions present during these periods helped to develop these stable boundary layers, the large-scale conditions were for the most part irrelevant to IOP operations.

“IOPs modulated by synoptic and mesoscale weather systems. IOP 1 (2–3 October) was intended to test operational procedures for the field program. Operations during the evening were conducted under clear skies with drainage flows developing as the evening progressed. However, a synoptic-scale northerly pressure gradient developed overnight to such an extent that northerly winds began to penetrate into the northern end of the Salt Lake Valley before midnight and eventually reversed the downvalley (southerly) flow through the center of the valley. Drainage circulations down into the valley from the Oquirrh and Wasatch Mountains were largely unaffected, however.

“IOPs 4 (8–9 October) and 7 (17–18 October) exhibited similar boundary layer structure to those in the first category until 0500 LST. Prior to that time, clear skies, weak winds aloft, and strong surface-based radiation inversions prevailed. As a result of approaching upper-level troughs from the west, however, the nocturnal inversions were then eroded in these two instances both by surface heating and by mixing due to the downward penetration of southerly winds from aloft.

“During IOPs 2 (6–7 October) and 3 (7–8 October), split flow aloft was present with weak upper-level short waves to the southwest and northeast of Utah. A strong outbreak of cold air to the east of the Continental Divide progressed westward on 6 October and overnight. By 0000 LST, easterly flow developed through gaps in the Wasatch Mountains and spilled through Parley’s Canyon into the Salt Lake Valley. At 0300 LST, the depth of the cold air to the east of the Wasatch Mountains built to sufficient height to spill over the lower terrain from Mill Creek Canyon to the area near the University of Utah in the northeast corner of the Salt Lake Valley and led to gusts in excess of 20 m s^{-1} that penetrated 1–2 km into the valley at the surface. These downslope wind conditions occur frequently along the Wasatch Mountains and the data collected during VTMX 2000 will provide considerable insight into their formation. The third IOP began at 1500 LST on 7 October and was terminated before midnight. Strong downslope winds persisted into the evening in the northeastern corner of the Salt Lake Valley and winds in the western part of the valley were too turbulent to permit tethered operations.

“Conditions during the last two IOPs (IOP 9: 20–21 October and IOP 10: 25–26 October) were affected significantly by approaching upper-level troughs. Both began in the afternoon with weak short-wave ridges overhead. Skies were broken to overcast and the strength of the nocturnal surface inversion and drainage circulations were weaker than those present during the other IOPs. A cold front entered the Salt Lake Valley at 0500 LST 21 October, ending operations during IOP 9. Southerly surface winds were enhanced during IOP 10 and provided favorable conditions for the final tracer release for the downtown region.

The following sections contain brief discussions of the wind regimes observed by the sonic anemometers and the integrated tower, sodar, and radar system at Raging Waters for each IOP. A composite of 30-min averages of wind speed, wind direction, virtual temperature, kinematic momentum flux, and kinematic sensible heat flux are shown for each IOP in Fig. 27.

IOP 1

Sonic Anemometers

Wind speed averaged about 0.5 m s^{-1} , which was about average for all the IOPs. Variability in 30-min average wind speed, as measured by the standard deviation at 0.25 m s^{-1} , was comparable to all other IOPs except for IOP5. Although the wind direction averaged about 170 deg, the greatest variability between all 30-min time periods was observed during this IOP. The highest average

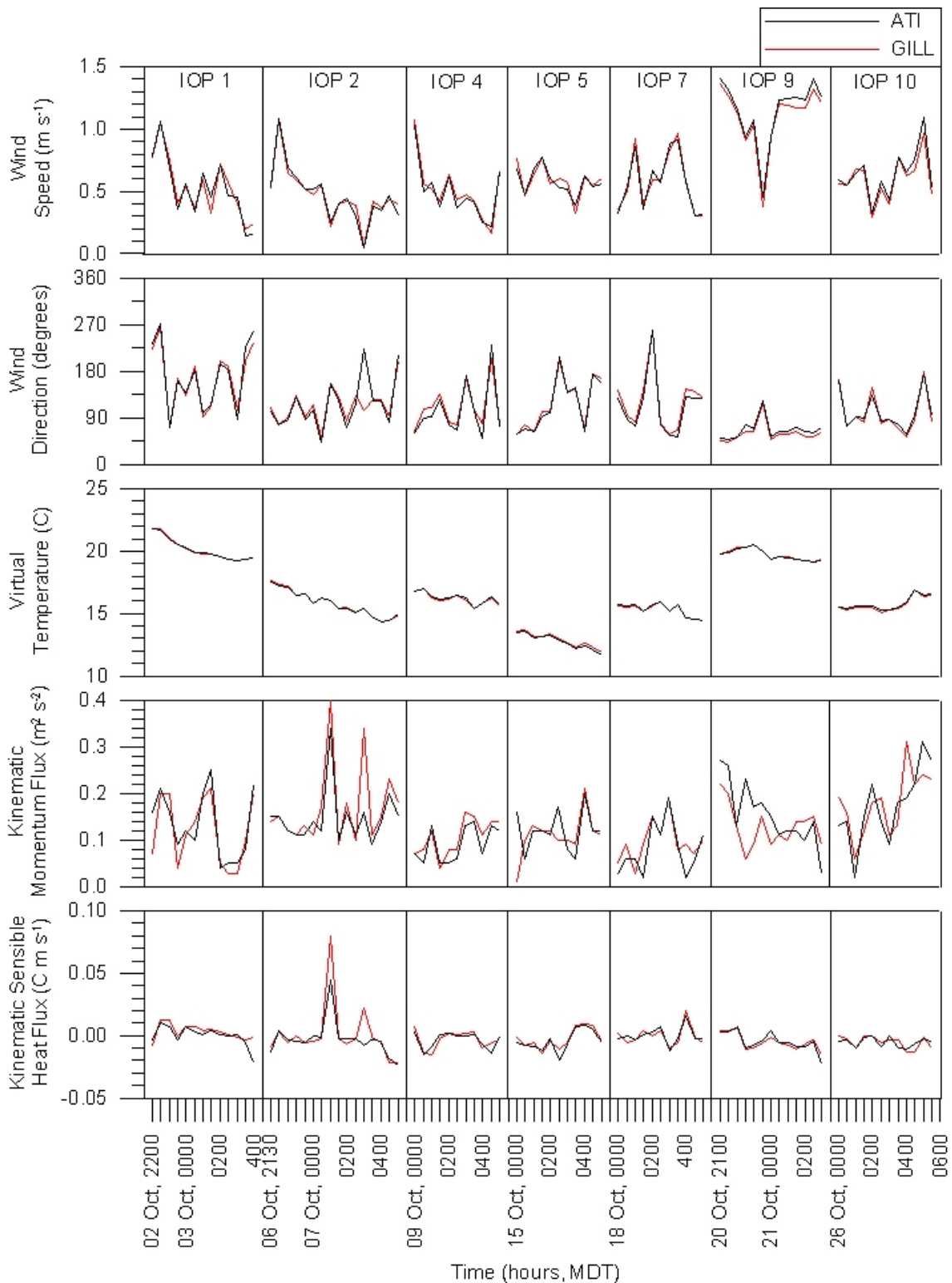


Figure 27. Sonic anemometer data averaged for 30-min time periods for wind speed, wind direction, virtual temperature, kinematic momentum flux, and kinematic sensible heat flux. Black is the ATI sonic anemometer and red is the Gill sonic anemometer.

virtual air temperature of any IOP was observed during this IOP at 20.1 °C. Kinematic momentum flux averaged $0.13 \text{ m}^2 \text{ s}^2$, and compared with IOPs 2, 9 and 10 in 30-min time period variability with a standard deviation of $0.07 \text{ m}^2 \text{ s}^2$. Average kinematic sensible heat flux was observed to be positive only during this IOP with a value of $0.0014 \text{ °C m s}^{-1}$. The standard deviation of this parameter was $0.0070 \text{ °C m s}^{-1}$, which was average for all IOPs except IOP 2.

Upper-air and Surface Meteorology

The 10-m tower, sodar, and radar were not operational during IOP 1.

IOP 2

Sonic Anemometers

Wind speed during IOP 2 averaged about 0.5 m s^{-1} , which was about average for all the IOPs. Variability in 30-min average wind speed, as measured by the standard deviation, was also comparable to most of the other IOPs at 0.22 m s^{-1} . The wind direction averaged about 115 deg, with a comparable standard deviation of 41 deg. The average virtual air temperature was 15.8 °C, but with the greatest standard deviation of any IOP at 1.0 °C. Kinematic momentum flux averaged $0.16 \text{ m}^2 \text{ s}^2$, and compared with IOPs 2, 9 and 10 in 30-min time period variability with a standard deviation of $0.07 \text{ m}^2 \text{ s}^2$. Kinematic sensible heat flux averaged near zero, but with a standard deviation that was about three times greater than that observed in any other IOP at $0.0190 \text{ °C m s}^{-1}$.

Upper-air and Surface Meteorology

Moderate winds were from the northwest from the surface up to about 300 m for the first couple of hours at the start of IOP 2 (Fig. 28). Light northerly winds were observed between 300 and 1000 m with light westerly winds above 1000 m. By 2000 MDT, the winds in the lowest several hundred meters became very light and variable. A shallow and weak southeasterly wind flow established itself from the surface up to 200 m after midnight with a modest easterly wind flow above 600 m. This weak southeasterly flow persisted until 0400 MDT. A strong easterly flow is observed beginning at this time between 250 m and 500 m. Over the next two hours, the easterly flow pushes down towards the surface. Very light southerly winds are found aloft above 1000 m during this strong low-level easterly flow. The easterly wind flow quickly shuts down within a 30-min period between 1030 and 1100 UTC near the end of the IOP. Winds from the surface up to 400 m become very light and variable.

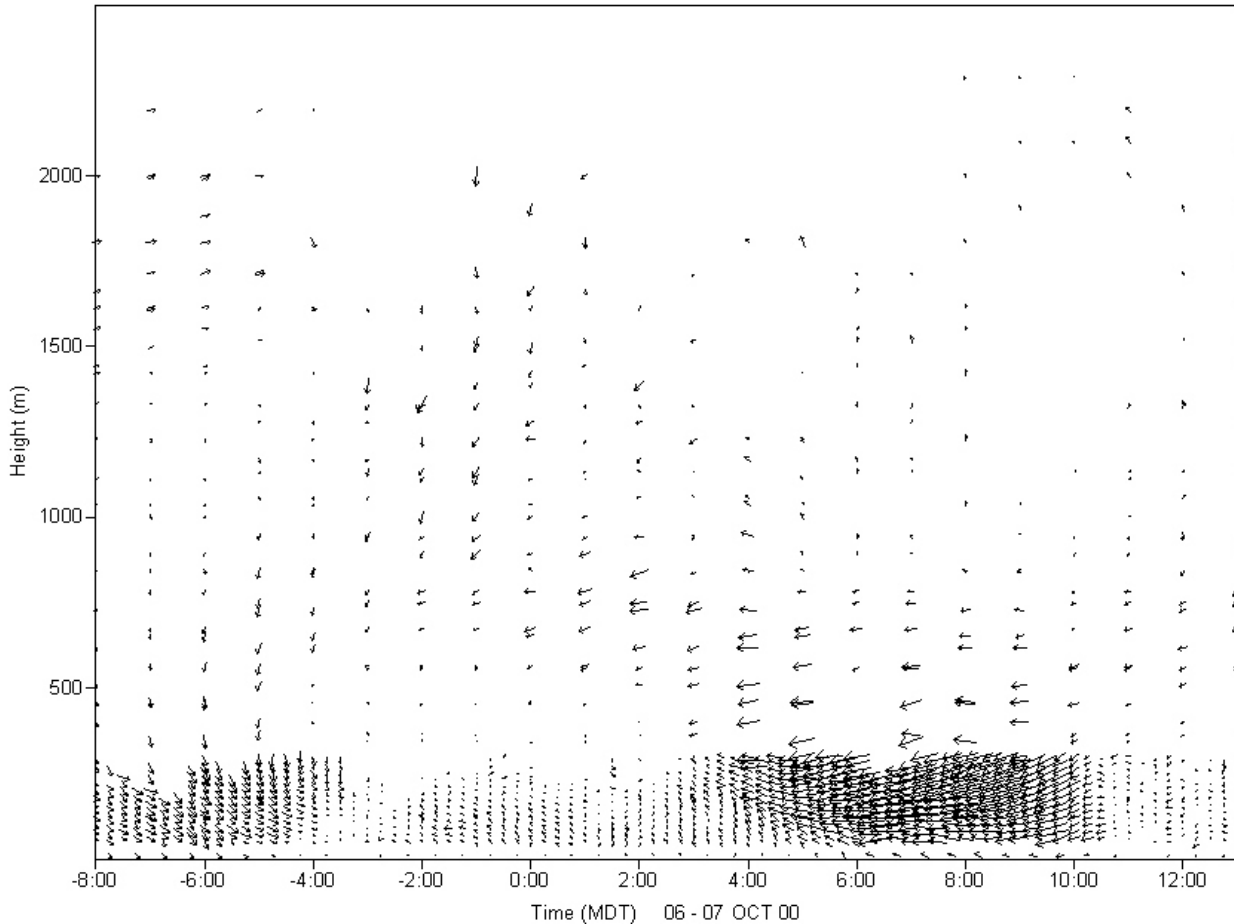


Figure 28. Tower, sodar, and radar wind vectors during IOP 2.

IOP 3

Sonic Anemometers

The two 3-D sonic anemometers were not used during IOP 3.

Upper-air and Surface Meteorology

The wind regime for IOP 3 (Fig. 29) is similar to that of IOP 2. Persistent northwesterly winds are found from the surface up to 300 m at the start of IOP 3 at 1600 MDT until 1900 MDT. A stronger northeasterly flow is found above that layer from 500 to 1000 m while very light southerly winds are found above 1000 m. By 2000 MDT, the northwesterly flow quickly breaks down and a strong northeasterly flow is established from the surface up to 500 m. For the next 10 to 12 hours, this northeasterly flow becomes more easterly in nature. By the next morning, this flow from the Wasatch mountains breaks down at the surface starting at 0900 MDT and is destroyed by 1000 MDT. For about an hour, the winds near the surface are light and variable before a weak

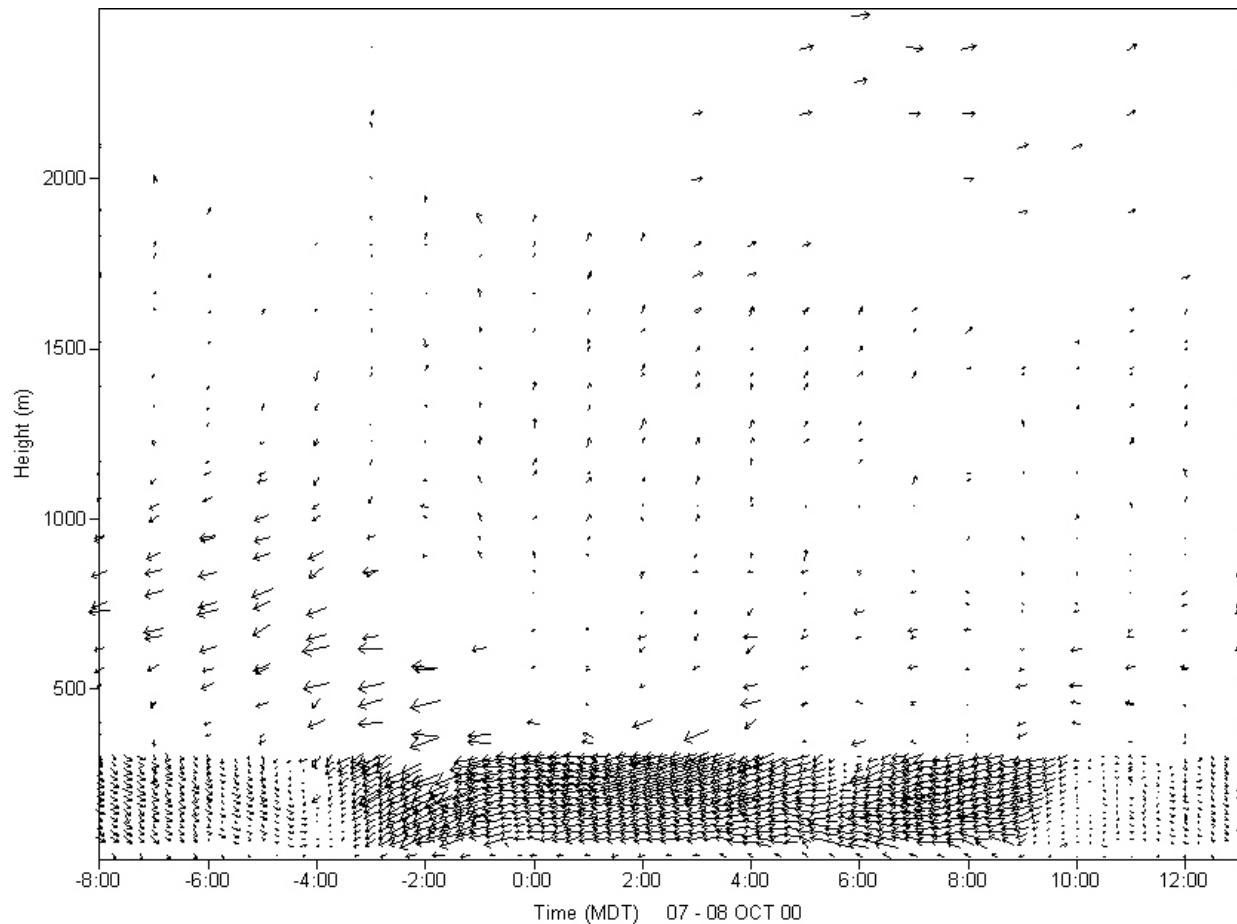


Figure 29. Tower, sodar, and radar wind vectors during IOP 3.

northwesterly flow from the surface up to 300 m establishes itself just prior to local noon. Note that a modest southwesterly flow is found above 1500 m during the last half of the IOP.

IOP 4

Sonic Anemometers

Wind speed during IOP 4 averaged about 0.5 m s^{-1} , again comparable to the experiment average. Wind speed standard deviation was also comparable to most of the other IOPs at 0.23 m s^{-1} . The wind direction averaged about 105 deg , with a standard deviation of 48 deg . The average virtual air temperature was $16.2 \text{ }^\circ\text{C}$. Kinematic momentum flux averaged $0.10 \text{ m}^2 \text{ s}^{-2}$ with a standard deviation of $0.04 \text{ m}^2 \text{ s}^{-2}$. Kinematic sensible heat flux averaged $-0.0033 \text{ }^\circ\text{C m s}^{-1}$, with a standard deviation of $0.0067 \text{ }^\circ\text{C m s}^{-1}$.

Upper-air and Surface Meteorology

A moderate northwesterly flow is observed from the surface to 300 m at the start IOP 4 beginning at 1600 MDT and lasting for about three hours (Fig. 30). A weak northerly flow is found above this wind flow from 500 to 1000 m while moderate southwesterly winds are observed above 1500 m. Between 1900 and 2200 MDT, the winds become light and variable from the surface up to 1000 m. However, by 2300 MDT, a weak southeasterly flow establishes itself from the surface up to 400 m with more southerly winds above 500 m. Over the next nine hours, this southeasterly flow slowly veers and eventually comes from the south. This southerly wind flow intensifies between 0800 and 1000 MDT, but then weakens during the last three hours of the IOP.

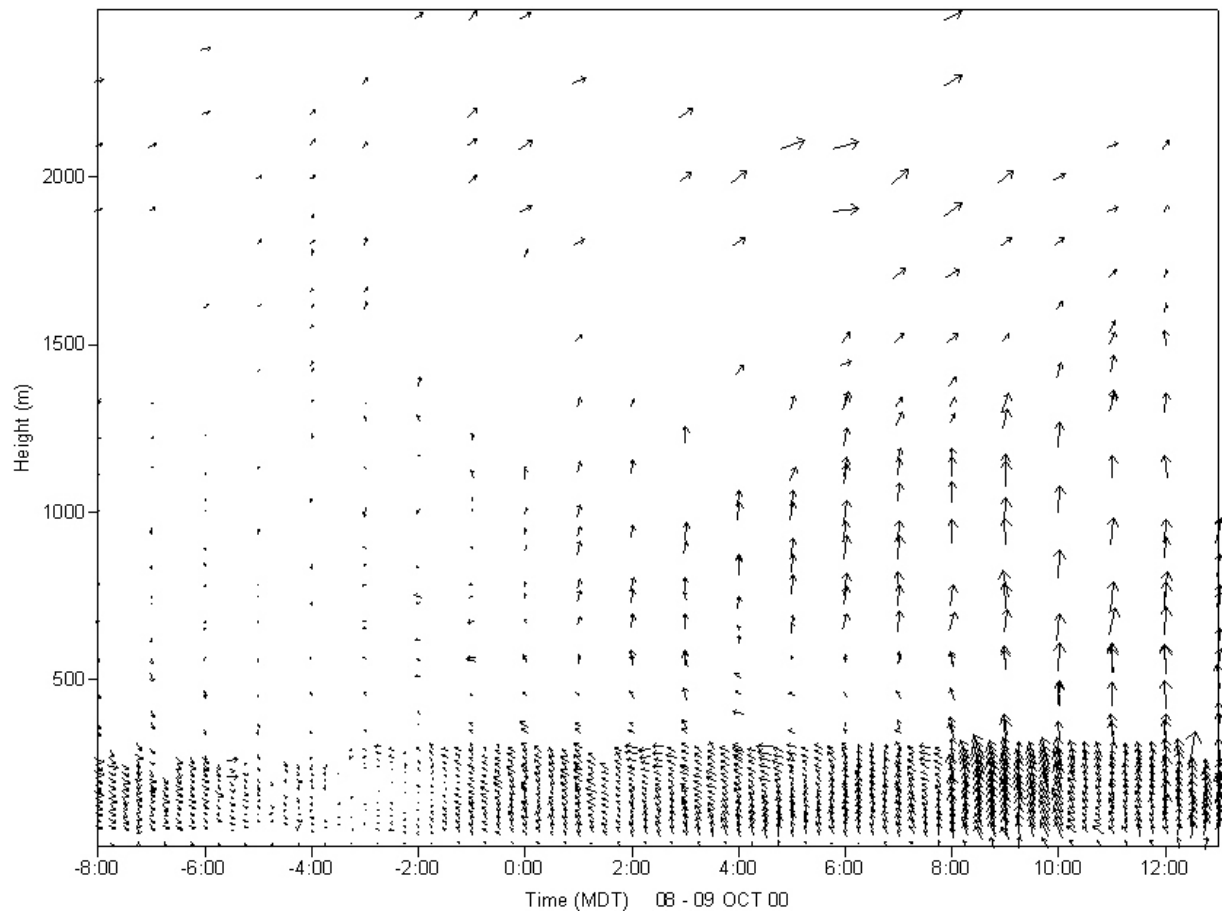


Figure 30. Tower, sodar, and radar wind vectors during IOP 4.

IOP 5

Sonic Anemometers

The parameters measured by the sonic anemometers during IOP 5 were essentially the same as for IOP 4.

Upper-air and Surface Meteorology

A very weak westerly to northwesterly flow is found for the first two hours of IOP 5 from the surface up to 1000 m (Fig. 31). Between 1800 and 2030 MDT, the winds are extremely light and variable throughout the sampling column. However, by 2030 MDT, a weak easterly wind flow establishes itself between the surface and 400 m. By 2300 MDT the flow veers and remains southeasterly until 0200 MDT. During this time period, moderate northwesterly to northerly winds are found aloft above 1000 m. Shortly after 0200 MDT, the winds become extremely light and variable from the surface up to 1000 m. The southeasterly wind flow reestablishes itself by 0400 MDT and lasts until 1000 MDT. For the last three hours of the IOP, the winds become extremely light and variable.

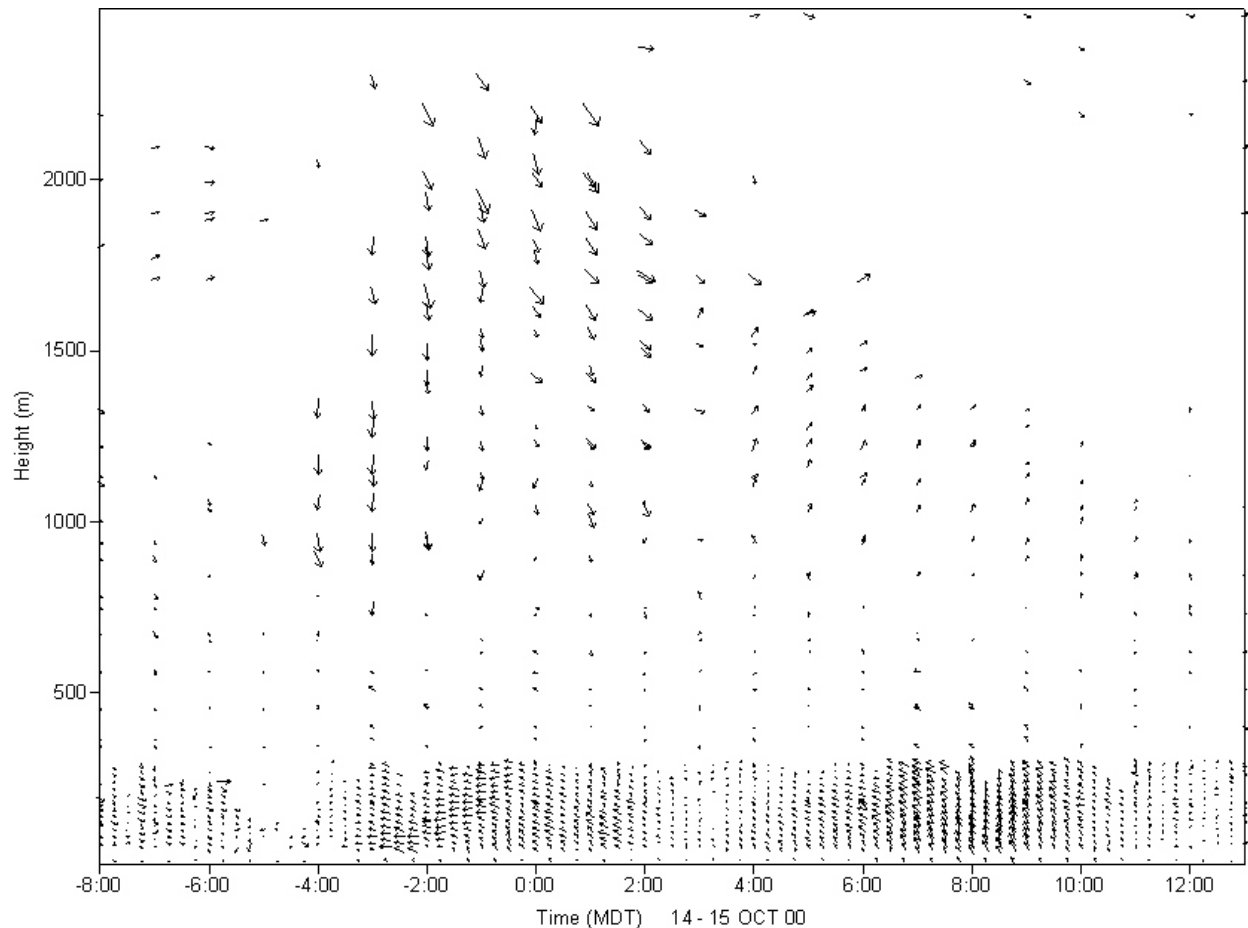


Figure 31. Tower, sodar, and radar wind vectors during IOP 5.

IOP 6

Sonic Anemometers

The two 3-D sonic anemometers were not used during IOP 6.

Upper-air and Surface Meteorology

Very light winds are found in IOP 6 (Fig. 32). Weak northwesterly to northerly winds are found for the first five hours of the IOP from 1600 to 2100 MDT from the surface up to 1000 m. The winds are light and variable for about one hour before a weak southeasterly flow establishes itself from the surface up to 400 m starting at 2200 MDT. The flow remains southeasterly from 2200 to 0200 MDT. The flow quickly becomes southerly after 0200 MDT. The southerly flow slowly decreases in magnitude over the next few hours until it becomes extremely light and variable after 1100 MDT. Winds above 500 m during IOP 6 are very light and show no particular organization.

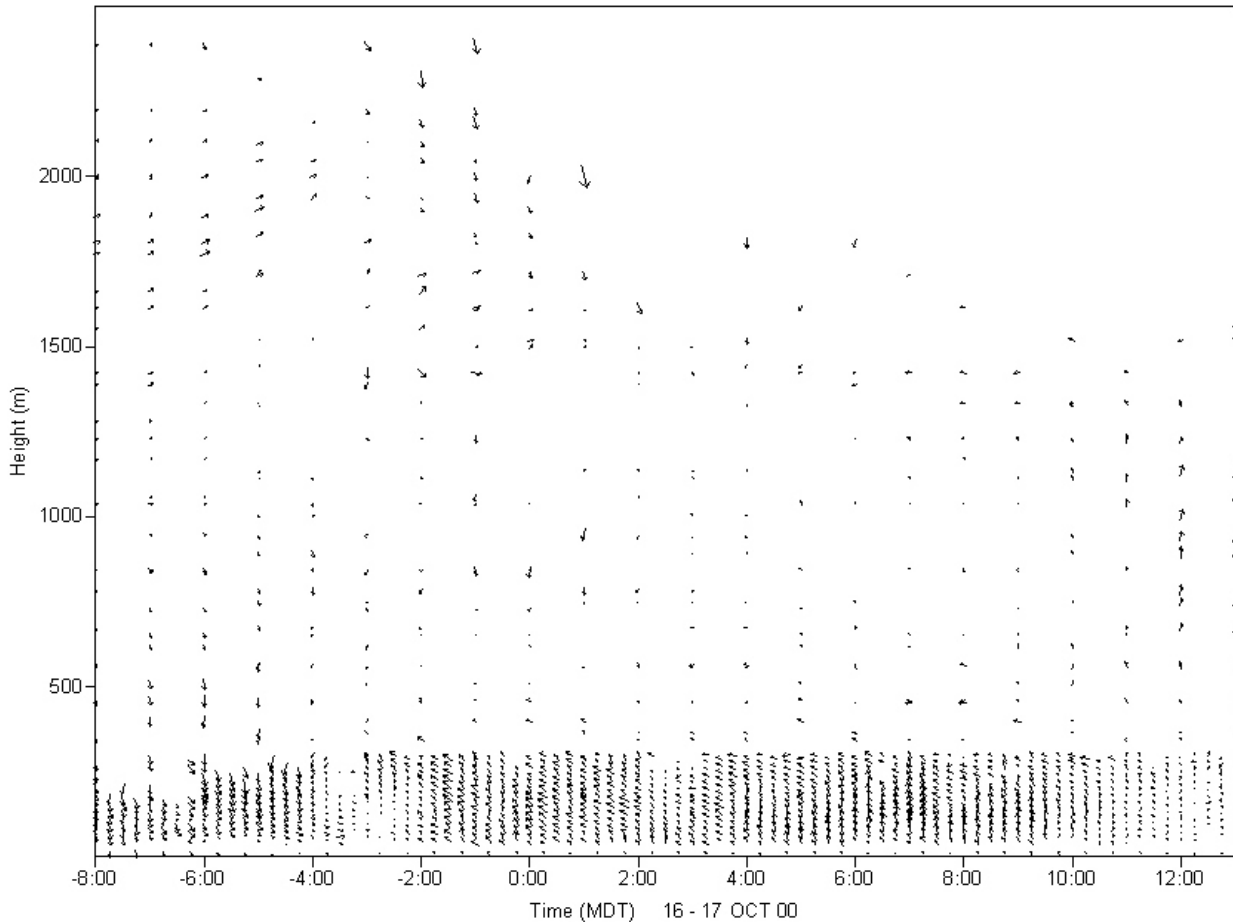


Figure 32. Tower, sodar, and radar wind vectors during IOP 6.

IOP 7

Sonic Anemometers

Wind speed during IOP 7 averaged about 0.6 m s^{-1} with a standard deviation of 0.23 m s^{-1} . The wind direction averaged about 118 deg, with a standard deviation of 55 deg. The average virtual air temperature was $15.3 \text{ }^\circ\text{C}$. Kinematic momentum flux averaged $0.09 \text{ m}^2 \text{ s}^{-2}$ with a standard deviation of $0.05 \text{ m}^2 \text{ s}^{-2}$. Kinematic sensible heat flux averaged almost zero with a standard deviation comparable to most of the other IOPs at $0.0073 \text{ }^\circ\text{C m s}^{-1}$.

Upper-air and Surface Meteorology

The low-level wind flow regime of IOP 7 (Fig. 33) is very similar to that found in IOP 6 except for stronger southerly to southwesterly winds found above 500 m. A weak northwesterly flow is observed from the surface up to 500 m from 1600 to 2000 MDT. The winds become extremely light and variable for two hours between 2000 and 2200 MDT but then become southeasterly after 2200 MDT from the surface up to 400 m. The southeasterly flow persists until

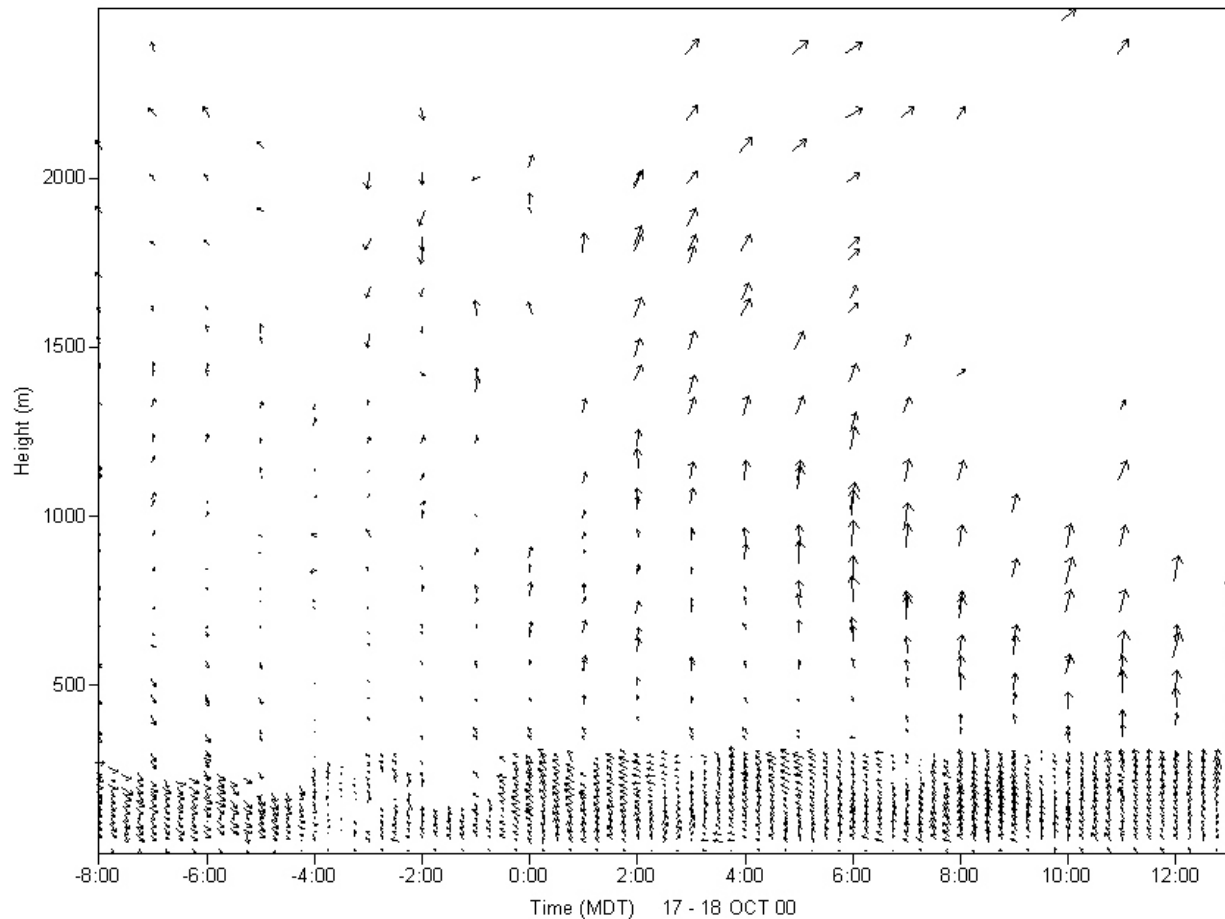


Figure 33. Tower, sodar, and radar wind vectors during IOP 7.

0200 MDT. For a short time, the winds in the first 300 m show a curious behavior. At 0230 MDT, the winds back with height from the southwest near the surface to the east at 300 m. Between 0430 and 0500 MDT a weak easterly flow is found at 300 m above a weak southerly flow. The winds remain light but from the south for the remainder of the IOP with a strong southerly wind flow found aloft between 500 and 1000 m. These shallow, but distinct wind regimes may be the interaction of two or more drainage flows originating from the canyons of the Wasatch Mountains. However, more detailed analysis in combination with other meteorological observations is needed before this assumption can be confirmed.

IOP 8

Sonic Anemometers

The two 3-D sonic anemometers were not used during IOP 8.

Upper-air and Surface Meteorology

Once again, the low-level flow features found in IOP 8 (Fig. 34) are very similar to those found in the previous two IOPs. A weak northwesterly to northerly flow is observed from 1600 to

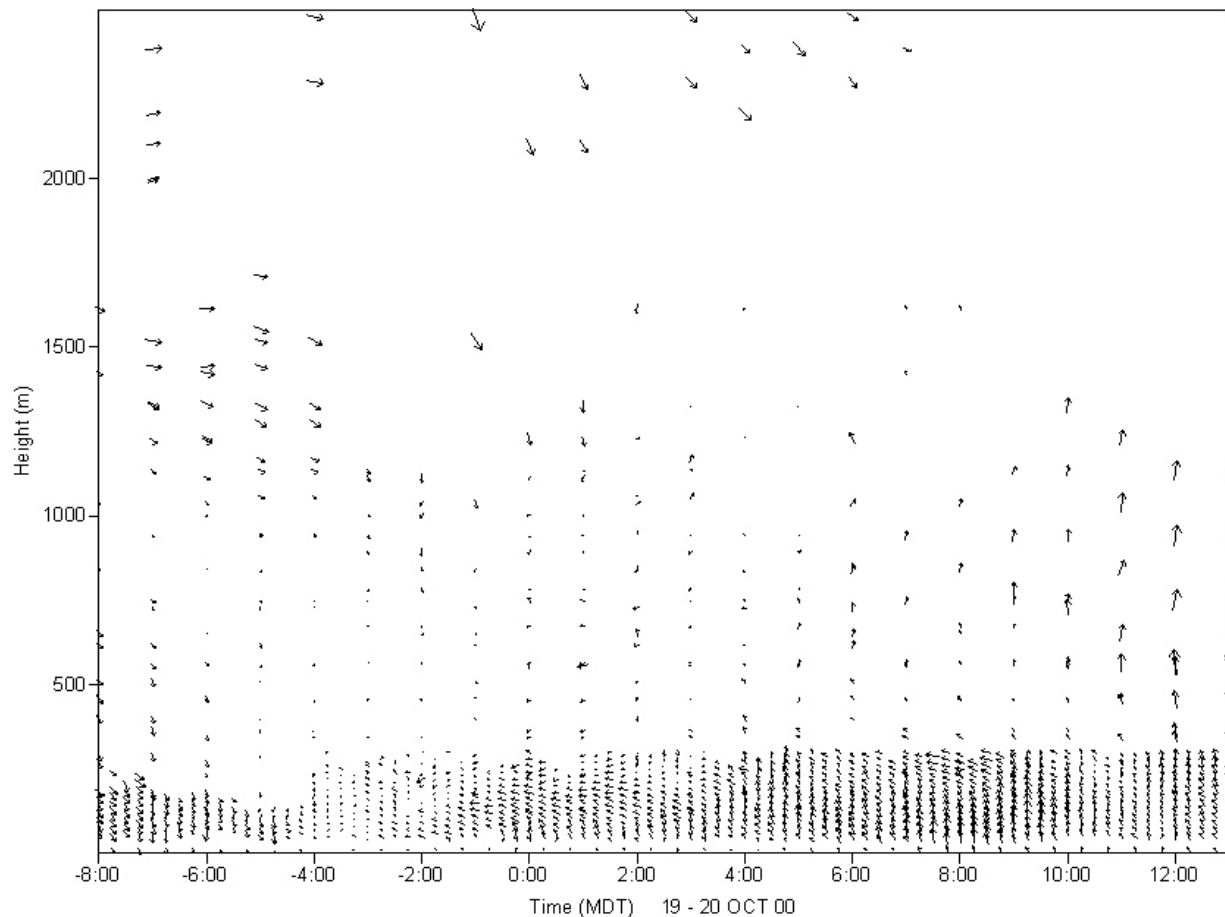


Figure 34. Tower, sodar, and radar wind vectors during IOP 8.

2000 MDT from the surface up to 1000 m. The winds become extremely light and variable between 2000 and 2200 MDT. A weak easterly flow begins to form around 2200 MDT which slowly veers to southeasterly over the next several hours. The southeasterly wind persists throughout the remainder of the IOP but weakens in the late morning hours between 1000 and 1200 MDT. A moderate northwesterly flow is observed above 2000 m during a portion of the IOP whereas flow between 500 and 1500 m was variable.

IOP 9

Sonic Anemometers

Average wind speed was about double for IOP 9 compared with the other IOPs. The average was 1.12 m s^{-1} , with a standard deviation of 0.25 m s^{-1} . The wind direction was also much different, with a east-northeasterly flow at 64 deg. All other IOPs exhibited wind flows from the southern quadrant. Average virtual temperature was the second highest of the IOPs at $19.7 \text{ }^\circ\text{C}$. Average kinematic momentum flux was $0.14 \text{ m}^2 \text{ s}^2$, very near the entire experimental average. Average kinematic sensible heat flux was the second highest negative of the IOPs at $-0.0047 \text{ }^\circ\text{C m s}^{-1}$.

Upper-air and Surface Meteorology

During this short IOP, the winds were rather strong and from the south from the surface up to 2000 m (Fig. 35). A weak southeasterly flow is observed in the first 50 m of the atmosphere from 2200 MDT to shortly after midnight. Very little variation is observed in the southerly wind regime.

IOP 10

Sonic Anemometers

Average wind speed during IOP 10 was about 0.6 m s^{-1} , which was second highest average of all IOPs. The standard deviation, was also comparable to most of the other IOPs at 0.18 m s^{-1} . The wind direction averaged about 100 deg, making the winds the most easterly of all IOPs. The wind direction standard deviation was 37 deg. The average virtual air temperature was $15.8 \text{ }^\circ\text{C}$ with a standard deviation of $0.5 \text{ }^\circ\text{C}$. Kinematic momentum flux averaged $0.18 \text{ m}^2 \text{ s}^2$, and compared with IOPs 1, 2, and 9 in 30-min time period variability with a standard deviation of $0.07 \text{ m}^2 \text{ s}^2$. Average kinematic sensible heat flux was the most negative of all IOPs at $-0.0054 \text{ }^\circ\text{C m s}^{-1}$ but with a standard deviation of $0.0040 \text{ }^\circ\text{C m s}^{-1}$.

Upper-air and Surface Meteorology

In this final IOP, the winds from the surface to the top of the sampling range have southerly components (Fig. 36). Light southerly winds for the first two hours of IOP 10 eventually become extremely light and variable from the surface up to 300 m. By 2100 MDT, a weak southeasterly

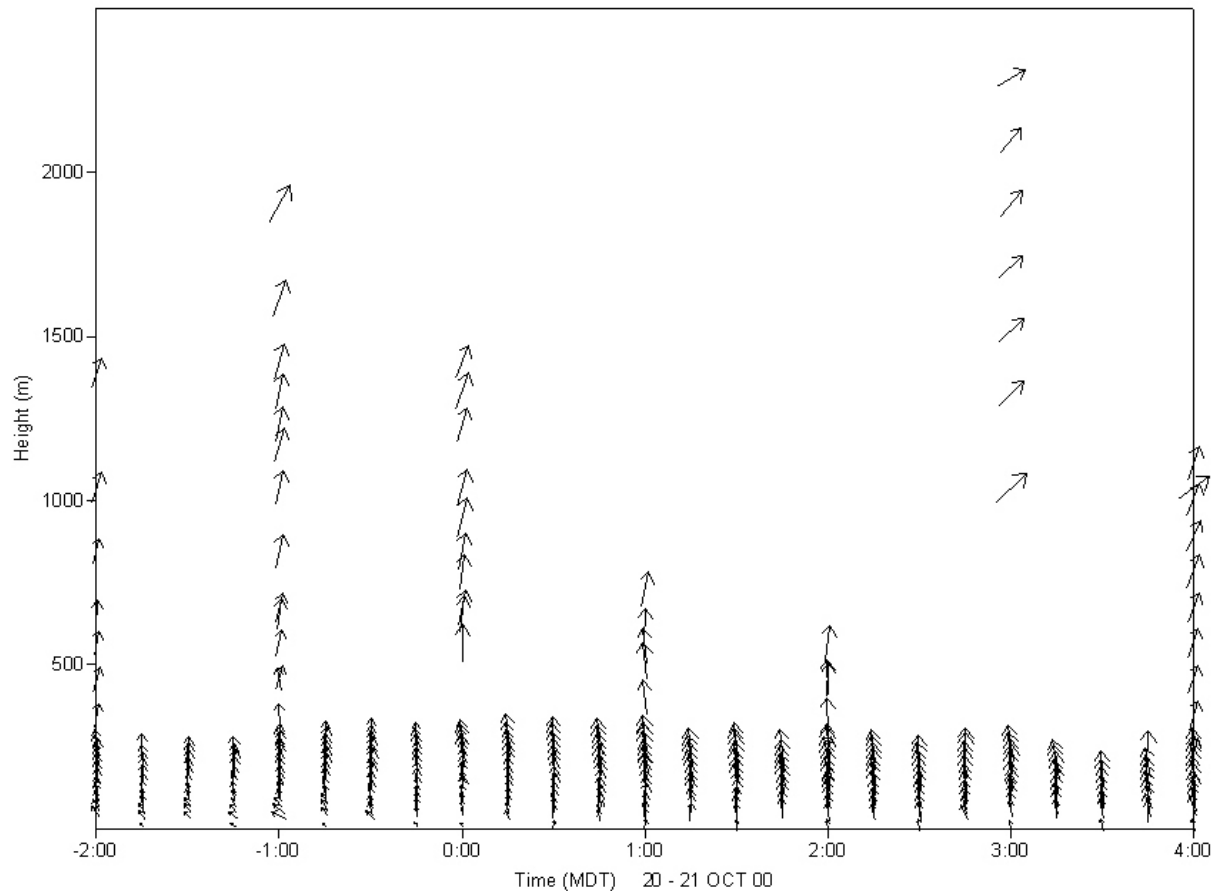


Figure 35. Tower, sodar, and radar wind vectors during IOP 9.

flow has established itself up to 300 m. The data show a dominant southerly flow of 4 to 5 m s⁻¹, repeatedly interrupted by southeasterly flow in a surface-based layer which deepens beyond 100 m and then subsides. Such encroachments were centered on 0030 MDT, 0300 MDT, 0600 MDT, and 0800 MDT. Between these episodes, the southerly flow reestablished itself all the way to the surface at 0130 MDT, 0500 MDT, and 0700 MDT. These data suggest an oscillating drainage flow. Aircraft data acquired in the eastern side of Salt Lake Valley sampled the event centered on 0600 MDT (Dobosy et al., 2002). An eastern north-south flight at 400 m AGL leg passed first above a drainage flow, then through the turbulent entrainment layer at its top, and finally within the drainage itself, characterized by northeast wind. The western north-south flight leg, farther into the valley shows only south winds, though there was drainage beneath, revealed in the now southeast flow reported by the tower, sodar, and radar.

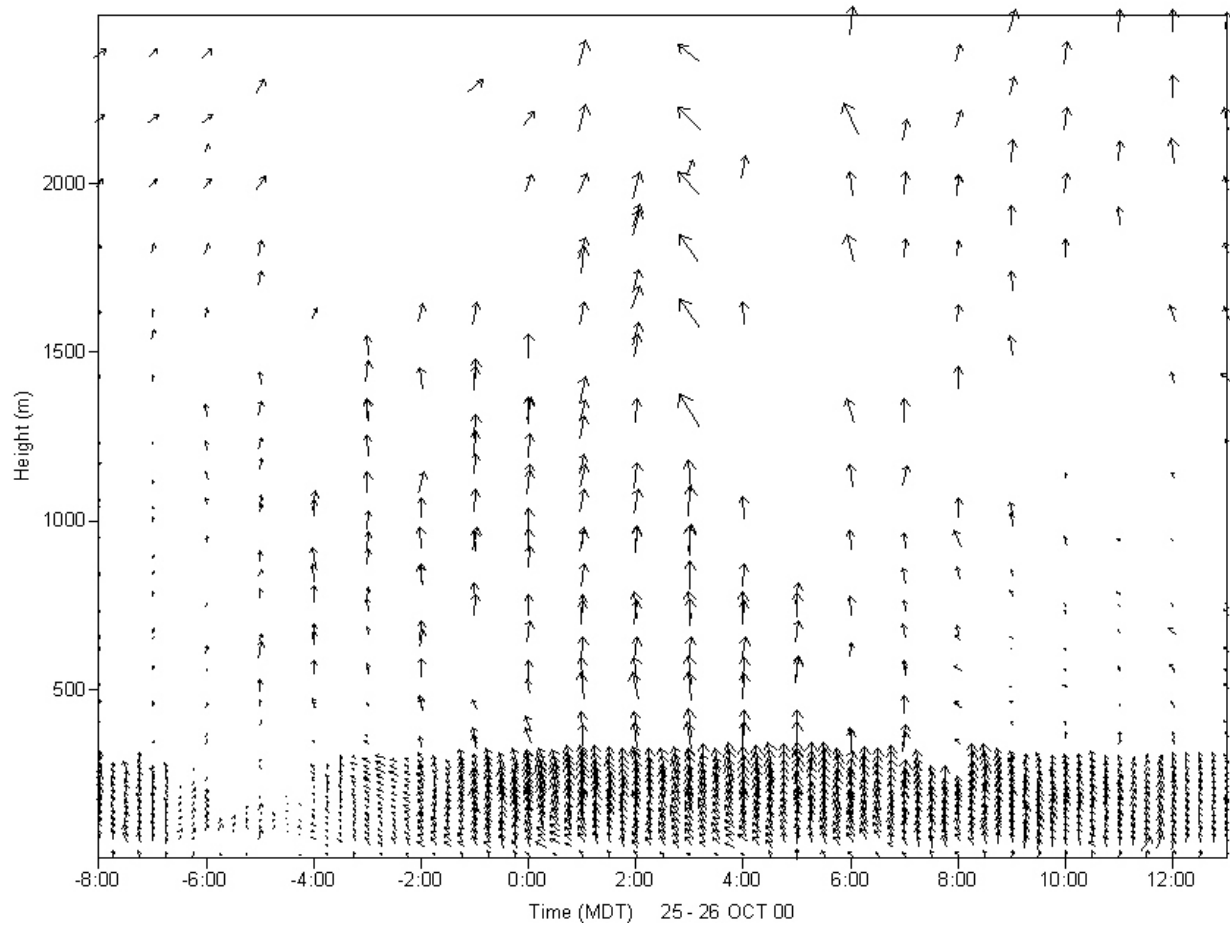


Figure 36. Tower, sodar, and radar wind vectors during IOP 10.

ACKNOWLEDGMENTS

The authors wish to thank Craig Curtis, General Manager of Raging Waters, for his permission to use Raging Waters for the surface and upper-air meteorological measurements during the URBAN 2000/VTMX field study. The authors wish to acknowledge the hard work of Tom Strong and Wayne Hooker for transporting the radar/sodar trailers from California upon the completion of the Central California Ozone Study (CCOS) to Salt Lake City and for their help setting up these measurements systems. Tom Strong and Shane Beard dismantled the Raging Waters site in the pouring rain at the completion of the study. The authors would also like to thank Neil Hukari for generating the wind rose plot for the Raging Waters 10-m tower. The thoughtful and insightful reviews of Ron Dobosy and Jason Ching are also appreciated.

URBAN 2000 was sponsored by the U. S. Department of Energy's Chemical and Biological National Security Program. VTMX was sponsored by the U. S. Department of Energy as part of the Environmental Meteorology Program.

REFERENCES

- Allwine, K. J., J. H. Shinn, G. E. Streit, K. L. Clawson, and M. Brown, 2002: An overview of URBAN 2000: A multi-scale field study of dispersion through an urban environment. *Bull. Amer. Meteor. Soc.*, **83**, 521-536.
- Crescenti, G. H., 1998: The degradation of Doppler sodar performance due to noise: A review. *Atmos. Environ.*, **32**, 1499-1509.
- Crescenti, G. H., and R. A. Baxter, 1998: Examples of noise interference on Doppler sodar performance. Preprint, *Tenth Symposium on Meteorological Observations and Instrumentation*, Phoenix, AZ, Amer. Meteor. Soc., 228-232.
- Dobosy, R. J., E. J. Dumas, and G. H. Crescenti, 2002: Katabatic flow and turbulence as seen from airborne in-situ measurements and ground-based profiler measurements during VTMX. Preprint, *Fourth Symposium on the Urban Environment*, Norfolk, VA, Amer. Meteor. Soc., paper 12.6.
- Doran, J. C., J. D. Fast, and J. Horel, 2002: The VTMX 2000 campaign. *Bull. Amer. Meteor. Soc.*, **83**, 537-551.
- Stull, R. B., 1988: *An Introduction to Boundary Layer Meteorology*. Kluwer Academic Press, Boston, MA, 666 pp.
- U. S. Department of Energy, 2001: *Chemical and Biological National Security Program 2000 Annual Report*. U. S. Department of Energy, 218 pp.
- U. S. Environmental Protection Agency, 1995: *Quality Assurance Handbook for Air Pollution Measurement Systems, Volume IV: Meteorological Measurements*. EPA-600/R-94-038d, Office of Research and Development, Research Triangle Park, NC, 280 pp.
- U. S. Environmental Protection Agency, 2000: *Meteorological Monitoring Guidance for Regulatory Modeling Applications*. EPA-454/R-99-005, Office of Air Quality Planning and Standards, Research Triangle Park, NC.
- Weber, B. L., and D. B. Wuertz, 1991: Quality control algorithm for profiler measurements of winds and temperatures. NOAA Technical Memorandum ERL WPL-212, Boulder, CO, 32 pp.
- Weber, B. L., D. B. Wuertz, D. C. Welsh, and R. McPeck, 1993: Quality controls for profiler measurements of winds and RASS temperatures. *J. Atmos. Oceanic Technol.*, **10**, 452-464.
- Wilczak, J. M., M. L. Cancillo, and C. W. King, 1997: A wind profiler climatology of boundary layer structure above the boreal forest. *J. Geophys. Res.*, **102**, 29083-29100.

This Page Intentionally Blank